

Feature Partition Aggregation: A Fast Certified Defense Against a Union of Sparse Adversarial Attacks

Zayd Hammoudeh* Daniel Lowd

University of Oregon

Abstract

Deep networks are susceptible to numerous types of adversarial attacks. Certified defenses provide guarantees on a model’s robustness, but most of these defenses are restricted to a single attack type. In contrast, this paper proposes feature partition aggregation (FPA) – a certified defense against a union of attack types, namely evasion, backdoor, and poisoning attacks. We specifically consider an ℓ_0 or sparse attacker that arbitrarily controls an unknown subset of the training and test features – even across all instances. FPA generates robustness guarantees via an ensemble whose submodels are trained on disjoint feature sets. Following existing certified sparse defenses, we generalize FPA’s guarantees to top- k predictions. FPA significantly outperforms state-of-the-art sparse defenses providing larger and stronger robustness guarantees, while simultaneously being up to $5,000\times$ faster.

Keywords: Certified classifier, sparse adversarial attack, ℓ_0 attack, evasion attack, data poisoning, backdoor attack

1 Introduction

Machine learning models are vulnerable to numerous types of adversarial attacks, including (1) *evasion attacks* which manipulate a model by perturbing test instances [Sze+14], (2) *poisoning attacks* which manipulate predictions by perturbing a model’s training set [BNL12], (3) *backdoor attacks* which combine training set and test perturbations [Li+22], and (4) *patch attacks* – a specialized evasion attack where the adversarial perturbation is restricted to a small contiguous region [Bro+17]. Most existing defenses against adversarial attacks are *empirical* [Mad+18] and “lack fundamental security rigor” [Kum+20]. Empirical defenses’ fatal weakness is that attacks can be (easily) adapted to bypass them [Tra+20].

In contrast, *certified defenses* provide a quantifiable guarantee of their effectiveness [LXL23]. Most certified defenses assume a single restricted threat model. However, in practice, adversarial attacks may be sourced from multiple threat models [TB19], making it imperative that critical ML systems are robust over a *union* of threat models simultaneously [SGF22].

To the extent of our knowledge, Weber et al. [Web+20] propose the only integrated defense that certifies robustness over the union of poisoning, backdoor, and evasion attacks. Their approach, based on randomized smoothing [CRK19], targets primarily an ℓ_2 attacker. The biggest limitation of Weber et al.’s defense is its minimal robustness guarantees – the equivalent of at most 10 arbitrarily perturbed pixels. In contrast, this work considers an ℓ_0 or “*sparse*” attacker that arbitrarily controls an unknown subset of the training and/or test features [Sch+19]. No bound is placed on the *poisoning rate*, meaning 100% of training instances may be adversarially perturbed. To our knowledge, this work is the first to provide non-trivial pointwise robustness guarantees over the union of evasion, poisoning, and backdoor attacks (sparse or otherwise), certifying predictions up to 1M arbitrarily perturbed feature values (e.g., pixels) across training and test.

Vertically partitioned datasets are particularly susceptible to this union of sparse attack types [Wei+22]. Vertical partitioning splits the feature set (i.e., data *columns*) across different silos (organizations), e.g., to preserve privacy in settings like healthcare [LDD21]. A single compromised vertical data source allows an attacker to *partially corrupt all instances* – training and test.

Existing certified ℓ_0 defenses use a custom randomized smoothing approach to prove sparse evasion robustness [LF20; Jia+22b]. In contrast, our certified sparse defense, *feature partition aggregation* (FPA), uses a model

*Correspondence to zayd@cs.uoregon.edu.

ensemble approach, where submodels are trained on disjoint feature subsets. Feature bagging has been used for decades to improve the accuracy of ensemble predictions, in particular with decision trees [Ho98]. Here, FPA uses disjoint feature bags to certify robustness against training and test feature perturbations.

Our primary contributions are listed below. Additional theoretical contributions and all proofs are in the supplement.

- We define a new robustness paradigm we term, *certified feature robustness* that generalizes sparse (ℓ_0) robustness to also encompass training set perturbations.
- We propose feature partition aggregation, which certifies feature robustness via an ensemble of submodels trained on disjoint feature sets.
- Following existing certified sparse defenses for recommender systems [Jia+22b], we generalize FPA to top- k predictions and propose a greedy algorithm that provides tight top- k guarantees. Our greedy algorithm can also certify top- k robustness for existing voting-based, certified classifiers.
- We empirically demonstrate that FPA outperforms state-of-the-art certified sparse defenses – providing larger and stronger certified robustness guarantees while also being 2 to 3 orders of magnitude faster.

2 Preliminaries

Notation Scalars and functions are denoted with lowercase italics letters. Vectors are denoted with lowercase bold letters. Matrices are denoted with uppercase bold letters; the j -th column of a matrix \mathbf{A} is denoted \mathbf{A}_j .¹

Let $[m]$ denote integer set $\{1, \dots, m\}$. $\mathbb{1}[a]$ is the *indicator function*, which equals 1 if predicate a is true and 0 otherwise. For any vector \mathbf{w} , ℓ_0 norm $\|\mathbf{w}\|_0$ is the number of non-zero elements in \mathbf{w} . In a slight abuse of notation, let $\mathbf{A} \ominus \mathbf{A}'$ denote the set of column *indices* over which two equal-size matrices \mathbf{A} and \mathbf{A}' differ. Formally,

$$\mathbf{A} \ominus \mathbf{A}' := \{j : \mathbf{A}_j \neq \mathbf{A}'_j\}. \quad (1)$$

Similarly, $\mathbf{v} \ominus \mathbf{v}'$ denotes the set of *dimensions* where vectors \mathbf{v} and \mathbf{v}' differ, meaning $\mathbf{v} \ominus \mathbf{v}' \subseteq [|\mathbf{v}|]$.

Let $\mathbf{x} \in \mathcal{X} \subseteq \mathbb{R}^d$ be a *feature vector* ($d := |\mathbf{x}|$) and $y \in \mathcal{Y} \subseteq \mathbb{N}$ a *label*. A *training set* $\{(\mathbf{x}_i, y_i)\}_{i=1}^n$ consists of n instances. Denote the training set’s *feature matrix* as $\mathbf{X} := [\mathbf{x}_1 \ \dots \ \mathbf{x}_n]^\top$ where $\mathbf{X} \in \mathbb{R}^{n \times d}$, and denote the label vector $\mathbf{y} := [y_1, \dots, y_n]$. Let $f : \mathcal{X} \rightarrow \mathcal{Y}$ be a *model*.

For feature partition aggregation (FPA), f is an ensemble of T *submodels*. Feature set $[d]$ is *partitioned* across the T submodels. Let $\mathcal{S}_t \subset [d]$ be the set of features used by submodel f_t where $\bigsqcup_{t=1}^T \mathcal{S}_t = [d]$. In other words, each submodel considers a fixed, disjoint subset of features from all training and test instances. Submodel f_t ’s training set D_t consists of the \mathcal{S}_t columns in \mathbf{X} and label vector \mathbf{y} . Submodels are *deterministic*, meaning provided fixed D_t , \mathcal{S}_t , and \mathbf{x} , prediction $f_t(\mathbf{x})$ is always the same.² Fig. 1 visualizes an example of our FPA ensemble architecture.

For any $\mathbf{x} \in \mathcal{X}$ and label $y \in \mathcal{Y}$, let

$$c_y(\mathbf{x}) := |\{t \in [T] : f_t(\mathbf{x}) = y\}| \quad (2)$$

be the number of submodels that predict label y for \mathbf{x} . Ensemble f ’s decision function is *voting-based* where for $\mathbf{x} \in \mathcal{X}$, the top-1 prediction is *plurality label* y_{pl} ,

$$f(\mathbf{x}) := y_{\text{pl}} = \arg \max_{y \in \mathcal{Y}} c_y(\mathbf{x}). \quad (3)$$

f ’s decision function generalizes to top- k prediction as

$$f(\mathbf{x}; k) := \arg \max_{\mathcal{Y}_k \subset \mathcal{Y}, |\mathcal{Y}_k|=k} \sum_{y \in \mathcal{Y}_k} c_y(\mathbf{x}). \quad (4)$$

All ties are broken by selecting the smallest class indices.

Threat Model Given k and arbitrary instance (\mathbf{x}, y) , the attacker’s objective is to ensure that $y \notin f(\mathbf{x}; k)$. The adversary achieves their objective via two possible methods: (1) modify training features \mathbf{X} and (2) modify test instance \mathbf{x} ’s features.³ An adversary may use either attack method individually or both methods jointly. The attacker has perfect knowledge of the learner and our method. No constraint is placed on an attack’s poisoning rate. An attacker can even (*partially*) *perturb 100% of the training instances*.

¹Supplemental Sec. A provides a nomenclature reference.

²A fixed random seed makes stochastic models deterministic.

³Our primary threat model assumes a *clean-label attacker* that does not modify training labels. Suppl. Sec. C provides additional theoretical results for an adversary that modifies training labels.

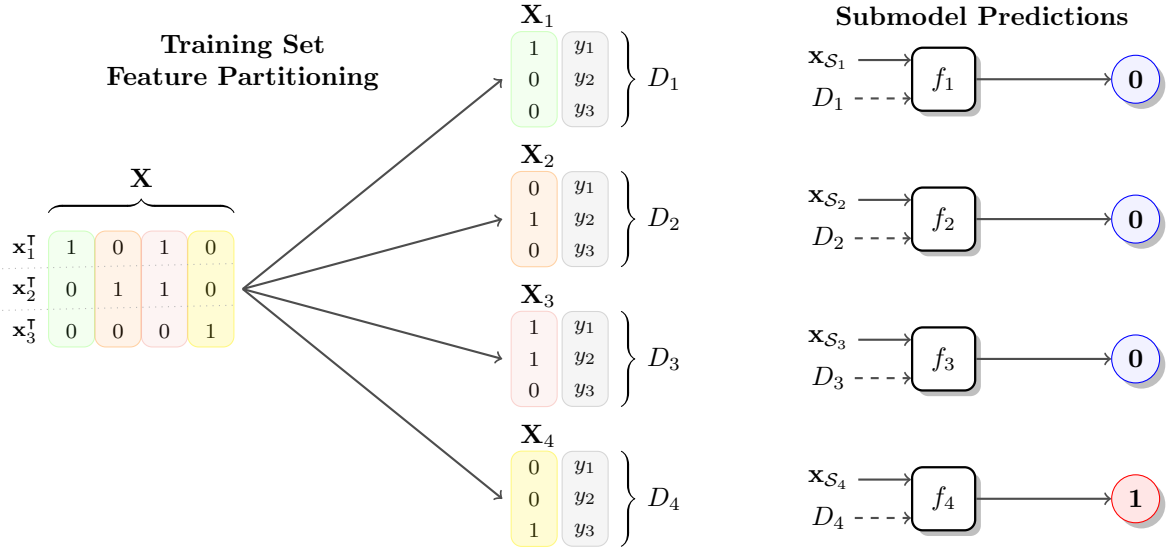


Figure 1: **Feature Partition Aggregation Overview** with $n = 3$ and $d = 4$. The feature set is partitioned across $T = 4$ submodels where $\forall t \in [T]$ submodel f_t uses only feature dimensions $\mathcal{S}_t = \{t\} \subset [4]$. Submodel f_t 's training set is D_t , i.e., the tuple containing the t -th column of feature matrix \mathbf{X} (denoted \mathbf{X}_t) and label vector $\mathbf{y} := [y_1, y_2, y_3]$. Given $\mathbf{x} \in \mathcal{X}$, let \mathbf{x}_{S_t} denote the preprocessed subvector of \mathbf{x} restricted to the feature dimensions in \mathcal{S}_t . Test prediction $f(\mathbf{x})$ has $c_0(\mathbf{x}) = 3$ and $c_1(\mathbf{x}) = 1$. Changing $f(\mathbf{x})$ requires changing at least two submodel predictions making the pointwise top-1 certified feature robustness $r = \lfloor \frac{3-1}{2} \rfloor = 1$ via Eq. (6).

Our Objective For arbitrary (\mathbf{x}, y) , determine the *certified feature robustness*, which we formalize below for $k \in \mathbb{N}$.

Def. 1. Top- k Certified Feature Robustness A pointwise, deterministic guarantee $r \in \mathbb{N}$ w.r.t. instance (\mathbf{x}, y) where for ensemble model f' trained on any training set $(\mathbf{X}', \mathbf{y})$ and evaluated on any instance $\mathbf{x}' \in \mathcal{X}$ s.t.

$$|\mathbf{X} \ominus \mathbf{X}' \cup \mathbf{x} \ominus \mathbf{x}'| \leq r \quad (5)$$

it holds that $y \in f'(\mathbf{x}'; k)$.

Observe that r is not w.r.t. feature values. Instead, r provides a stronger guarantee allowing all values of a feature – training and test – to be perturbed. *Pointwise* guarantees certify each instance (\mathbf{x}, y) individually.

3 Related Work

To the extent of our knowledge, this is the first work to propose certified feature robustness. Feature partition aggregation (FPA) marries ideas from two classes of certified adversarial defenses, which are discussed below.

ℓ_0 -Norm Certified Evasion Defenses First, representing the most closely related work, these defenses certify ℓ_0 -norm robustness – a strictly weaker guarantee than certified feature robustness. Def. 2 formalizes ℓ_0 -norm robustness for top- k predictions. Note that ℓ_0 -norm robustness is also referred to as *sparse robustness*.

Def. 2. Top- k ℓ_0 -Norm Certified Robustness A pointwise, probabilistic guarantee $\rho \in \mathbb{N}$ w.r.t. instance (\mathbf{x}, y) such that $\forall \mathbf{x}' \in \mathcal{X}$ where $\|\mathbf{x} - \mathbf{x}'\|_0 \leq \rho$, $y \in f(\mathbf{x}'; k)$.

There are two primary differences between the certified guarantees in Def. 1 and Def. 2. (1) ℓ_0 -norm defenses are not robust against any adversarial training perturbations (poisoning). (2) ℓ_0 -norm robustness guarantees are *probabilistic*, while Def. 1's feature guarantees are deterministic.

State-of-the-art certified ℓ_0 -norm defenses are based on *randomized ablation* (RA) – a specialized form of randomized smoothing [CRK19] for sparse evasion attacks [LF20]. RA creates a *smoothed classifier* by repeatedly evaluating

different *ablated inputs*, each of which *keeps* a small random subset of the features unchanged and masks out (*ablates*) all other features. Like all smoothing-based methods, RA performs smoothing (i.e., ablation) during training and inference. RA’s *ablated training* generally permits only stochastically-trained, parametric model architectures. At inference, certifying a single prediction with RA requires evaluating up to 100k randomly ablated inputs [Jia+22b].

Recently, Jia et al. [Jia+22b] improved RA’s guarantees via certification analysis that is tight for top-1 predictions and almost tight for $k > 1$. Jia et al.’s improved version of RA serves as our primary baseline since its performance is provably at least as good as the original version of RA.

Certified patch robustness is a weaker form of ℓ_0 -norm robustness specific to vision where the perturbed test features are assumed contiguous and a specific shape, e.g., 5×5 pixels [Xia+21; MY21]. Any certified ℓ_0 -norm or certified feature defense is also a certified patch defense, given the former’s stronger guarantees.

Certified Poisoning Defenses The second class of related defenses certifies robustness under the arbitrary insertion or deletion of entire *instances* in the training set – generally a small poisoning rate (e.g., $< 2\%$). Like FPA, most certified poisoning defenses are voting-based [Jia+22a; WLF22]. For example, *deep partition aggregation* (DPA) randomly partitions the training *instances* across an ensemble of T submodels [LF21]. By training submodels on disjoint sets of instances, DPA certifies robustness w.r.t. entire training instances. While certified poisoning defenses show promise, they are still vulnerable to test perturbations – even of a single feature.

4 Certifying Feature Robustness

Our certified sparse defense, feature partition aggregation (FPA), can be viewed as the *transpose* of Levine and Feizi’s [LF21] deep partition aggregation (DPA). Both defenses are (1) ensembles, (2) rely on voting-based decision functions, and (3) partition the training set. The key difference is in the partitioning operation. DPA partitions the set of training instances (*rows* of feature matrix \mathbf{X}) while our method, FPA, partitions the set of features (*columns* of \mathbf{X}). Under feature partitioning, each feature affects at most one submodel prediction (“vote”). We leverage this property to certify feature robustness r . Below, we first derive FPA’s top-1 robustness, where r has a closed form. We then generalize FPA to top- k predictions, where our greedy algorithm finds a tight, worst-case bound.⁴

4.1 Certifying a Top-1 Prediction

Recall from Sec. 2 that top-1 prediction $f(\mathbf{x})$ is the plurality label in multiset $\{f_t(\mathbf{x}) : t \in [T]\}$, with ties broken by selecting the label with the smaller index. Since each submodel f_t is trained on a disjoint feature set, controlling a single feature – training or test – gives an attacker control of at most one submodel’s “vote.” For an attack to succeed, the attacker must control sufficient votes to change the ensemble’s plurality label (y_{pl}). The minimum number of submodel “votes” that must change is half the vote-count difference between the plurality and runner-up labels. Thm. 3 formalizes this insight as a robustness guarantee, where indicator function $\mathbb{1}[\cdot]$ is needed to break ties. Thm. 3’s bound r is deterministic and tight in the worst case. Eq. (6)’s overall form is similar to other voting-based certified defenses [LF21; Jia+22a].

Theorem 3. Top-1 Certified Feature Robustness *Given submodel feature partition S_1, \dots, S_T , let f be a voting-based ensemble of T submodels, where each submodel f_t uses only the features in S_t . Then the pointwise top-1 certified feature robustness of prediction $y_{\text{pl}} = f(\mathbf{x})$ is*

$$r = \left\lfloor \frac{c_{y_{\text{pl}}}(\mathbf{x}) - \max_{y' \neq y_{\text{pl}}} (c_{y'}(\mathbf{x}) + \mathbb{1}[y' < y_{\text{pl}}])}{2} \right\rfloor. \quad (6)$$

Understanding Thm. 3 More Intuitively Let $\mathcal{A}_{\text{tr}} \subseteq [d]$ be the set of features (i.e., dimensions) an attacker modified in the training set, and let $\mathcal{A}_{\text{x}} \subseteq [d]$ be the set of features the attacker modified in $\mathbf{x} \in \mathcal{X}$. As long as $|\mathcal{A}_{\text{tr}} \cup \mathcal{A}_{\text{x}}| \leq r$, the adversarial perturbations did not change model prediction $f(\mathbf{x})$. The union over the perturbed feature sets entails that a feature perturbed in both training and test counts only once against guarantee r . Put simply, there is no double counting of a perturbed feature. Thm. 3’s certified guarantees are implicitly agnostic to the (sparse) attack type. Certified feature robustness r applies equally to a sparse evasion attack (\mathcal{A}_{x} only) as it does to sparse poisoning (\mathcal{A}_{tr} only). Thm. 3’s guarantees also encompass more complex backdoor attacks ($\mathcal{A}_{\text{tr}} \cup \mathcal{A}_{\text{x}}$).

Complexity FPA top-1 certification requires $\mathcal{O}(T)$ time.

⁴Additional theoretical contributions are in suppl. Secs. C & D

Algorithm 1 Top- k Greedy Robustness Certification

Input: Instance $\mathbf{x} \in \mathcal{X}$; target label $y \in \mathcal{Y}$; $k \in \mathbb{N}$; label vote counts

$$\forall_{y' \in \mathcal{Y}} c_{y'}(\mathbf{x})$$

Output: Certified feature robustness r

```

1:  $r \leftarrow -1$ 
2: while  $c_y(\mathbf{x})$  is in the top  $k$  do
3:    $\tilde{y} \leftarrow$  Label with the  $(k + 1)$ -th most votes
4:   if  $c_y(\mathbf{x}) > 0$  then
5:      $c_y(\mathbf{x}) \leftarrow c_y(\mathbf{x}) - 1$ 
6:   else
7:      $y_{\text{pl}} \leftarrow \arg \max_{y'} c_{y'}(\mathbf{x})$  ▷ Plurality label
8:      $c_{y_{\text{pl}}}(\mathbf{x}) \leftarrow c_{y_{\text{pl}}}(\mathbf{x}) - 1$ 
9:      $c_{\tilde{y}}(\mathbf{x}) \leftarrow c_{\tilde{y}}(\mathbf{x}) + 1$ 
10:     $r \leftarrow r + 1$  ▷ Update certified robustness
11: return  $r$ 

```

4.2 Certifying a Top- k Prediction

In line with Jia et al.’s [Jia+22b] extension of randomized ablation to top- k certification, we generalize FPA to top- k predictions below. For simplicity of presentation, we restrict consideration to the meaningful case where $k < T$.

Implicitly, Thm. 3’s certified robustness r quantifies the number of “votes” (submodel predictions) that can switch from plurality label y_{pl} to the runner-up label without changing prediction $f(\mathbf{x})$. The simplicity of top-1 predictions permits Eq. (6)’s neat closed form. Thm. 3’s guarantee r can also be calculated greedily, where “votes” are switched, one at a time, from y_{pl} to the runner-up label with the transfer stopping right before $f(\mathbf{x})$ changes. While top- k feature robustness does not have a convenient closed form like Eq. (6), an (optimal) greedy strategy still applies.

Intuitively, a label y is not in the top k if there exist k labels with more votes. Hence, two approaches to eject y from the top k are: (1) Reduce $c_y(\mathbf{x})$, the number of submodels that predict y . (2) Increase the number of votes for \tilde{y} , i.e., the label with $(k + 1)$ -th most votes. Our greedy, top- k certification algorithm applies these two approaches simultaneously by iteratively switching submodel predictions from y to \tilde{y} . Note that for $k > 1$, label \tilde{y} may change after each greedy iteration; it is this interaction that complicates providing a compact closed-form top- k guarantee r .

Alg. 1 formalizes the above intuition into a complete method to calculate top- k certified feature robustness r . With linear-time sorting (e.g., counting sort), Alg. 1 has $\mathcal{O}(T)$ time complexity – same as top-1 certification.⁵

Theorem 4. Top- k Greedy Strategy Optimality *Alg. 1 returns top- k certified feature robustness r that is tight under worst-case perturbations.*

Alg. 1 addresses an edge case to ensure r is tight. Based on how ties are broken, a label y can be in the top k without receiving any votes (i.e., $c_y(\mathbf{x}) = 0$). In such cases, Alg. 1 transfers votes from plurality label y_{pl} . Perturbing y_{pl} ensures $c_{\tilde{y}}(\mathbf{x})$ is monotonically increasing. Like \tilde{y} , y_{pl} can change between loop iterations.

Generalizing our Top- k Greedy Algorithm Observe that Alg. 1 deals only in vote counts (i.e., $c_{y'}(\mathbf{x})$) and is agnostic to how these independent votes are generated – be it over partitioned features or otherwise. Multiple existing certified defenses (e.g., deep partition aggregation [LF21] and the nearest neighbor-based poison defense [Jia+22a]) are top-1 only and voting-based, with the votes independent. Alg. 1 can be directly reused to generalize these existing certified defenses to provide robustness guarantees over top- k predictions. Alg. 1 also applies to alternate FPA formulations with non-pristine training labels (see suppl. Sec. C).

Accuracy-Robustness Tradeoff For partitioning-based certified defenses, there exists an implicit tradeoff between the number of partitions and the maximum achievable robustness. Fewer partitions generally result in better accuracy but lower peak robustness; more partitions reduce accuracy but increase peak robustness. FPA is no exception to this rule as Lem. 5 proves where T is the partition count.

⁵With a more sophisticated greedy strategy, certifying a top- k prediction requires no more than $\mathcal{O}(k)$ greedy iterations. We provide the less efficient Alg. 1 here for simplicity. Our source code implements both greedy algorithms.

Lemma 5. For any voting-based classifier with T submodels trained on partitioned feature sets, the top- k certified feature robustness satisfies $r \leq \left\lceil \frac{kT}{k+1} \right\rceil$ when $1 \leq k < T$.

Rule of Thumb: Given k and target robustness r_{target} , we empirically observe that the optimal submodel count (T) is usually around $\left\lceil \frac{k+1}{k} r_{\text{target}} \right\rceil$.

4.3 Advantages of Feature Partition Aggregation

To conclude, we summarize FPA’s advantages over ℓ_0 -norm certified defenses, e.g., randomized ablation.

- (1) **Stronger Guarantees** FPA’s certified feature robustness guarantee (Def. 1) is strictly stronger than RA’s ℓ_0 -norm guarantee (Def. 2). First, FPA’s guarantees apply equally to sparse evasion, poisoning, and backdoor attacks while RA is evasion only. Second, FPA’s guarantees are deterministic, with RA’s guarantees only probabilistic.
- (2) **Faster** RA requires up to 100k forward passes to certify one prediction. FPA requires only T forward passes – one for each submodel – where $T < 150$ in general. FPA is, therefore, orders of magnitude faster than RA.
- (3) **Model Architecture Agnostic** Smoothing-based methods like RA are generally limited to stochastically-trained model architectures. RA cannot directly leverage non-stochastic models like gradient-boosted decision trees. By contrast, FPA supports any submodel architecture.

5 Feature Partitioning Strategies

The certification analysis above holds irrespective of the feature partitioning strategy. This statement should not be interpreted to mean that all feature partitions are equally good. The way features are partitioned can have a *major* impact on the level of robustness that can be certified.

5.1 Properties of a Good Feature Partition

Since the feature partition dictates information flow to each submodel, we look to information theory to gain insights into what makes one feature partition better than another. We very briefly describe two of these insights below.

Insight #1 *Ensure sufficient information is available to each submodel.* For voting-based decisions, each incorrect “vote” cancels out a correct one, meaning the goal should be to both maximize the number of correct submodel predictions and minimize incorrect ones. In other words, robustness is maximized when all submodels perform well, and feature information is divided equally.

Insight #2 *Limit information loss due to feature partitioning.* Feature partitioning is lossy from an information theoretic perspective. Fixing T , some partitions are more lossy than others, and good partitions limit the information loss.

5.2 Feature Partitioning Paradigms

Applying these insights, we propose two general feature partitioning paradigms below. In practice, the partitioning strategy is essentially a hyperparameter and tunable on validation data. The validation set need not be clean as long as the perturbations are representative of the test distribution.

Balanced Random Partitioning Given no domain-specific knowledge, each feature’s expected information content is equal. *Balanced random partitioning* assigns each submodel a disjoint feature subset sampled uniformly at random, with subsets differing in size by at most one. Random partitioning has two primary benefits. First, each submodel has the same a priori expected information content. Second, random partitioning can be applied to any dataset. FPA with random partitioning is usually a good initial strategy and empirically performs quite well.

Deterministic Partitioning One may have application-related insights into quality feature partitions. For example, consider feature partitioning of images. Features (i.e., pixels) in an image are ordered, and that structure can be leveraged to design better feature partitions. Often the most salient features are clustered in an image’s center. To ensure all submodels are high-quality, each submodel should be assigned as many highly salient features as possible. Moreover, adjacent pixels can be highly correlated, i.e., contain mostly the same information. Given a fixed set of pixels to analyze, the information contained in those limited features should be maximized, so a good strategy can be to select a set of pixels spread uniformly across the image. Put simply, for images, random partitioning can have larger information loss than deterministic strategies. Suppl. Sec. F.5 empirically compares random and deterministic partitioning. In short, a simple *strided* strategy that distributes features regularly across an image tends to work well for vision. Formally, given d pixels and T submodels, submodel f_t ’s feature set under strided partitioning is $\mathcal{S}_t = \{j \in [d] : j \bmod d = t\}$.

5.3 Beyond Partitioned Feature Subsets

Everything above should *not* be interpreted to imply that certifying feature robustness necessarily requires partitioned feature sets. Submodel feature sets can partially overlap, but determining optimal r under overlapping sets is NP-hard in general via reduction to (partial) set cover. FPA’s computational efficiency is an important strength over methods like randomized ablation (Sec. 6.3). Tying FPA to an NP-hard optimization destroys this differentiator. Nonetheless, suppl. Sec. D extends FPA to overlapping feature sets and provides an empirical comparison. In summary, overlapping feature sets can marginally outperform random partitioning but often lags deterministic partitions.

6 Evaluation

Below, we empirically evaluate our certified defense, feature partition aggregation. Due to space, most experimental results are in the supplement, including: base (uncertified) accuracy for each evaluated dataset (F.1), full certified accuracy plots (F.2), hyperparameter sensitivity analysis (F.3 & F.4), random vs. deterministic partitioning comparison (F.5), and model training times (F.6).

6.1 Experimental Setup

Due to space, most evaluation setup details are deferred to supplemental Sec. E with a brief summary below.⁶

Baselines Randomized ablation (RA) is FPA’s most closely related work and serves as the primary baseline below. We used Jia et al.’s [Jia+22b] improved version of RA that provides robustness guarantees at least as large as the original. RA performs feature ablation during both training and inference. Each ablated input keeps e randomly selected features unchanged and masks out the remaining $(d - e)$ features; RA evaluates up to 100,000 ablated inputs to certify one prediction. Hyperparameter e controls RA’s accuracy vs. robustness tradeoff, where smaller e increases the maximum ℓ_0 -norm certified robustness but decreases overall accuracy. Recall that baseline RA’s ℓ_0 -norm robustness (Def. 2) is strictly weaker than FPA’s certified feature robustness (Def. 1). Put simply, a true direct comparison is not possible here since FPA provides stronger certified guarantees than the baseline.

We also briefly compare FPA to two certified patch defenses – *interval bound propagation* [Chi+20b] and BAGCERT [MY21].

Performance Metric *Certified accuracy* w.r.t. $\psi \in \mathbb{N}$ quantifies the fraction of correctly-classified test instances with certified robustness at least ψ .

Datasets We focus on the standard datasets used in data poisoning evaluation. For classification, we consider MNIST ($d = 784$) and CIFAR10 ($d = 1024$)⁷ where each feature corresponds to one (RGB) pixel in line with previous work. Following Jia et al.’s [Jia+22b] RA evaluation, we report certified accuracy for top 1, 2, and 3 predictions.

So far, this paper has discussed exclusively certified classification. Hammoudeh and Lowd [HL23] prove that certified regression *reduces* to voting-based certified classification when median is used as a model’s primary decision function. In short, certified classifiers like FPA and RA can be transformed into certified regressors via a simple change to the classifiers’ decision function.⁸ We apply Hammoudeh and Lowd’s reduction, and following Hammoudeh and Lowd’s empirical evaluation, we consider two tabular regression datasets. (1) Weather [Mal+21] predicts ground

⁶Source code: <https://github.com/ZaydH/feature-partition>.

⁷Existing certified poisoning defenses do not evaluate on full ImageNet due to the high training cost [LF21; Jia+22a; WLF22; Web+20].

⁸Sec. E.6 details the regression to classification reduction.

temperature within $\pm 3^\circ\text{C}$ using features such as date, time, longitude, and latitude ($d = 128$). (2) Ames [De 11] predicts housing prices within $\pm 15\%$ of their actual selling price using features such as square footage and number of bedrooms ($d = 352$). We chose these two regression datasets as a stand-in for vertically partitioned data, which are commonly tabular and, as Sec. 1 mentions, particularly vulnerable to our union of sparse attack types.

Model Architectures For MNIST and CIFAR10, FPA and RA used convolutional neural networks. For regression, the model choice is more nuanced. While FPA is model architecture agnostic, RA’s ablated training prevents it using statically trained models like gradient-boosted decision trees (GBDTs). GBDTs work exceptionally well on tabular (regression) data [BHL22]. As such, FPA used LightGBM GBDTs [Ke+17] for Weather and Ames, while RA used a linear model (Hammoudeh and Lowd [HL23] also used a linear model for Weather).⁹

The regression to voting-based classification reduction assumes that the total number of “votes” is odd. Hence, submodel count T is odd-valued for Weather and Ames.

Feature Partitioning Strategy For CIFAR10 and MNIST, strided feature partitioning was used, and each submodel considered the full image dimensions with any pixels not in \mathcal{S}_t set to 0. For Weather and Ames, balanced random partitioning was used as the tabular features are unordered.

Hyperparameters Recall that FPA’s hyperparameter T and baseline RA’s hyperparameter e control each method’s tradeoff between accuracy and robustness. In practice, T and e can be tuned on validation data to find the optimal hyperparameter setting for each certified robustness value. Such tuning significantly increases the methods’ training cost for often just modest performance gains. For reference, Sections F.3 and F.4 visualize in detail the effect of T and e (respectively) on each method’s certified accuracy.

Due to limited space, the next section considers only two hyperparameter settings per method for each dataset. Specifically, we report the certified accuracy with (1) a hyperparameter setting that provides higher accuracy and (2) a hyperparameter setting that provides better peak robustness. For feature partition aggregation, smaller T provides better accuracy while larger T provides better peak robustness. For baseline randomized ablation, the opposite is true where larger e provides better accuracy and smaller e provides better peak robustness. For CIFAR10 and MNIST, we report e values that Levine and Feizi [LF20] observed provided strong median certified robustness. For Weather and Ames, e was tuned on held-out data. FPA’s submodel count T was tuned on held-out data for all four datasets.

6.2 Main Results

Figs. 2 and 3 visualize the results for classification and regression, respectively. To reduce clutter, these figures always report the best performing of the two RA hyperparameter settings (e) for each certified robustness value (x-axis). The transition point between the two RA e settings (i.e., high accuracy and better peak robustness) is marked with a dotted, gray vertical line (---). At this vertical dotted line, FPA’s results also switch between the high accuracy and better robustness T settings. In short, the hyperparameter transition points in Figs. 2 and 3 were chosen to be optimal for baseline RA given the two e settings.

We briefly summarize these experiments’ takeaways below.

Takeaway #1 *On all four datasets, FPA consistently provides comparable or better robustness.* Importantly, FPA’s certified feature guarantees apply to evasion, poisoning, and backdoor attacks, while the baseline RA only covers evasion attacks. In short, FPA provides additional dimensions of robustness essentially for free.

Takeaway #2 *FPA’s certified accuracy and maximum certified robustness are significantly larger than the baseline for CIFAR10, Weather, and Ames.* FPA’s maximum certified robustness (x-axis) is nearly $2\times$ larger than RA for CIFAR10. For Weather and Ames, FPA’s maximum robustness is 50% and 33% larger (resp.). Moreover, FPA’s certified accuracy (y-axis) is up to 29% and 26% percentage points better than RA for CIFAR10 and Weather (resp.). The performance gains are on top of FPA’s stronger robustness guarantees. The gains span data modalities and model architectures, demonstrating FPA’s generality.

Takeaway #3 *FPA provides strong patch robustness without any assumptions about patch shape.* FPA with $T = 115$ certifies 34.7% of top-1 CIFAR10 predictions up to $r = 25$ perturbed pixels (2.4% of d) – training or test. For comparison, state-of-the-art patch defenses *interval bound propagation* [Chi+20b] and BAGCERT [MY21] certify 30.3% and 60.0% (resp.) of CIFAR10 predictions under specifically a 5×5 pixel test-only patch attack (not shown

⁹FPA with linear models also outperforms randomized ablation (see Secs. F.2.3 & F.2.4).

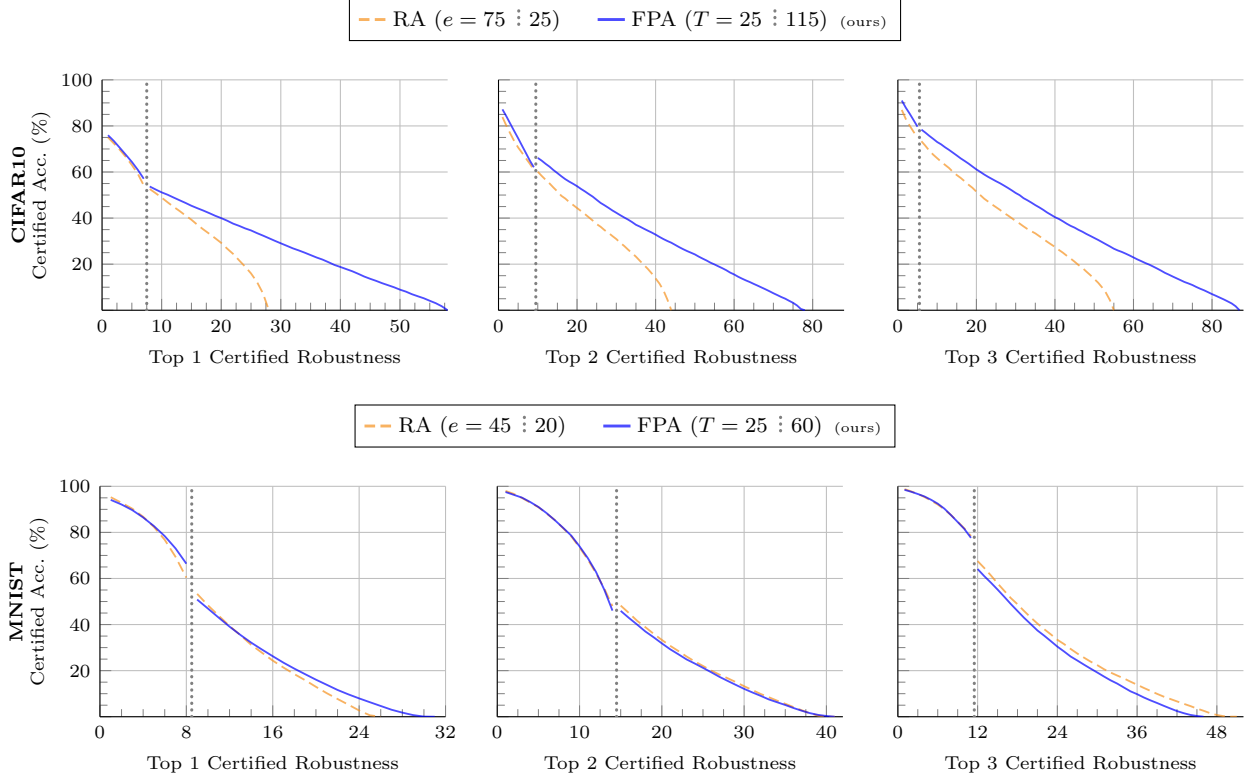


Figure 2: **Classification Certified Accuracy:** Comparison of feature partition aggregation (FPA: —) vs. baseline randomized ablation (RA: -- --) for CIFAR10 ($d = 1024$) and MNIST ($d = 784$). Sec. 6.1 explains that two hyperparameter settings are used per method for each dataset. A vertical, dotted line (\cdots) marks the certified robustness value (x-axis) where the hyperparameter settings transition from higher accuracy to better robustness. Each dataset’s hyperparameter settings are listed in the corresponding legend where ($e = 75 \div 25$) denotes $e = 75$ is used on the left of the dotted line and $e = 25$ used on the line’s right, with a similar notation for T . For CIFAR10, FPA has stronger and larger robustness guarantees than the baseline. For MNIST, FPA slightly outperforms RA for top-1, and both methods perform similarly for top-2. For complete, detailed results, see Secs. F.2.1 and F.2.2. See Tab. 17 for the base (uncertified) accuracies.

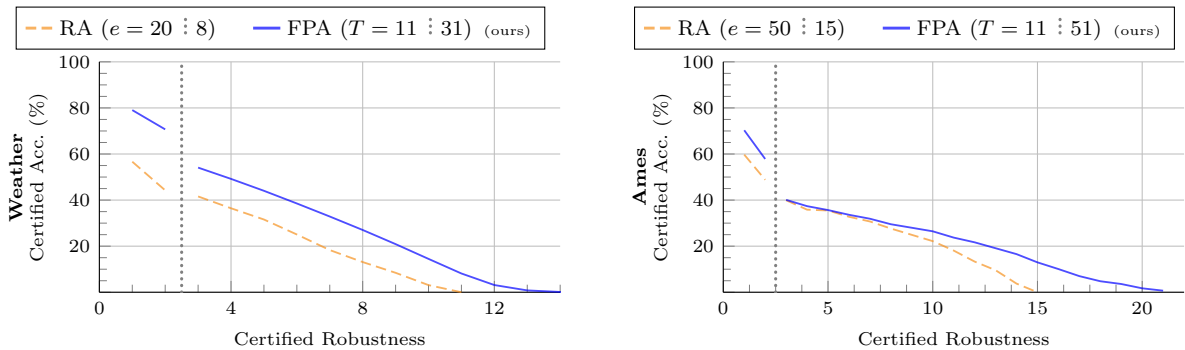


Figure 3: **Regression Certified Accuracy:** Comparison of feature partition aggregation (—) vs. baseline randomized ablation (-- --) for Weather ($d = 128$) and Ames ($d = 352$). Sec. 6.2 summarizes the takeaways. For complete results, see suppl. Secs. F.2.3 and F.2.4. Top- k does not apply to regression.

Table 1: **Certification Time:** Comparison of the mean time (in seconds) to certify a single prediction using FPA and randomized ablation. FPA is 2 to 3 orders of magnitude faster than baseline RA. We report the certification time for only FPA’s largest T values, meaning these values are FPA’s minimum speedup over RA.

| Dataset | Random. Abl. | | FPA _(ours) | | Speedup |
|---------|--------------|--------|-----------------------|--------|---------|
| | e | Time | T | Time | |
| CIFAR10 | 25 | 4.7E+0 | 115 | 7.2E-3 | 652× |
| MNIST | 20 | 6.5E-1 | 60 | 2.7E-3 | 243× |
| Weather | 8 | 6.8E-1 | 31 | 1.3E-4 | 5,231× |
| Ames | 15 | 3.2E-1 | 51 | 5.5E-4 | 582× |

in Fig. 2). Recall that certified patch defenses provide weaker guarantee than even ℓ_0 -norm robustness (Def. 2) since patch defenses assume the perturbed test pixels are a specific contiguous shape (generally a square). Patch guarantees may not hold under: (1) multiple patches, (2) training perturbations, or (3) alternate patch shapes (e.g., BAGCERT’s CIFAR10 certified accuracy drops to $\sim 40\%$ for 24×1 patches). While less effective than dedicated patch defenses that make stronger assumptions and weaker guarantees, FPA is still competitive, providing patch guarantees for free.

Takeaway #4 *FPA is the first integrated defense to provide significant pointwise robustness guarantees over the union of evasion, backdoor, and poison attacks.* Consider CIFAR10 ($n = 50,000$); feature robustness $r \geq 25$ certifies a prediction’s robustness against 1.25M arbitrarily perturbed pixels. In contrast, the only other certified defense robust over the union of evasion, backdoor, and poisoning attacks [Web+20] certifies the equivalent of 3 or fewer arbitrarily perturbed CIFAR10 pixels (i.e., a total training and test ℓ_2 perturbation distance of ≤ 3). Going further, FPA certifies $r \geq 7$ for 32.5% of Weather predictions ($n > 3M$) – a pointwise guaranteed robustness of up to 21M arbitrarily perturbed feature values.

6.3 Certification Time

Jia et al.’s [Jia+22b] improved version of RA evaluates 100k ablated inputs to certify each prediction. In contrast, feature partition aggregation requires exactly T forward passes per prediction (one per submodel). Table 1 compares the mean certification time for FPA and RA. We report the certification time for FPA’s largest T values only, meaning Tab. 1 represents our worst-case speedup.

Speedup Takeaway FPA certifies predictions 2 to 3 orders of magnitude faster than baseline RA.

7 Conclusions

This paper proposes *feature partition aggregation* – a certified defense against a union of sparse attack types. FPA outperforms the state-of-the-art sparse defense providing both larger and stronger robustness guarantees. FPA is also more flexible – supporting any submodel architecture – and 2 to 3 orders of magnitude faster. FPA’s certified feature guarantees are particularly important for *vertically partitioned data* where a single compromised data source allows an attacker to arbitrarily modify a limited number of (tabular) features for all instances – training and test.

To the extent of our knowledge, FPA is the first integrated defense to provide non-trivial pointwise robustness guarantees against the union of evasion, poisoning, and backdoor attacks – sparse or otherwise [Web+20]. Future work remains to develop effective certified defenses over this union of attack types for alternate ℓ_p threat models.

Acknowledgments

The authors thank Jonathan Brophy for helpful discussions and feedback on earlier drafts of this manuscript. This work was supported by a grant from the Air Force Research Laboratory and the Defense Advanced Research Projects Agency (DARPA) — agreement number FA8750-16-C-0166, subcontract K001892-00-S05, as well as a second grant from DARPA, agreement number HR00112090135. This work benefited from access to the University of Oregon high performance computer, Talapas.

References

- [Bar17] Jonathan T. Barron. *Continuously Differentiable Exponential Linear Units*. 2017. arXiv: 1704.07483 [cs.LG]. URL: <https://arxiv.org/abs/1704.07483>.
- [BNL12] Battista Biggio, Blaine Nelson, and Pavel Laskov. “Poisoning Attacks against Support Vector Machines”. In: *Proceedings of the 29th International Conference on Machine Learning*. ICML’12. Edinburgh, Great Britain: PMLR, 2012. URL: <https://arxiv.org/abs/1206.6389>.
- [BHL22] Jonathan Brophy, Zayd Hammoudeh, and Daniel Lowd. *Adapting and Evaluating Influence-Estimation Methods for Gradient-Boosted Decision Trees*. 2022. arXiv: 2205.00359 [cs.LG]. URL: <https://arxiv.org/abs/2205.00359>.
- [Bro+17] Tom B. Brown, Dandelion Mané, Aurko Roy, Martín Abadi, and Justin Gilmer. *Adversarial Patch*. 2017. arXiv: 1712.09665 [cs.CV]. URL: <http://arxiv.org/abs/1712.09665>.
- [Che+17] Xinyun Chen, Chang Liu, Bo Li, Kimberly Lu, and Dawn Song. *Targeted Backdoor Attacks on Deep Learning Systems Using Data Poisoning*. 2017. arXiv: 1712.05526 [cs.CR]. URL: <https://arxiv.org/abs/1712.05526>.
- [Chi+20a] Ping-yeh Chiang, Michael J. Curry, Ahmed Abdelkader, Aounon Kumar, John Dickerson, and Tom Goldstein. “Detection as Regression: Certified Object Detection by Median Smoothing”. In: *Proceedings of the 34th Conference on Neural Information Processing Systems*. NeurIPS’20. Virtual Only: Curran Associates, Inc., 2020. URL: <https://arxiv.org/abs/2007.03730>.
- [Chi+20b] Ping-yeh Chiang, Renkun Ni, Ahmed Abdelkader, Chen Zhu, Christoph Studor, and Tom Goldstein. “Certified Defenses for Adversarial Patches”. In: *Proceedings of the 8th International Conference on Learning Representations*. ICLR’20. Virtual Only, 2020. URL: <https://openreview.net/forum?id=HyeaSkryPH>.
- [CRK19] Jeremy Cohen, Elan Rosenfeld, and Zico Kolter. “Certified Adversarial Robustness via Randomized Smoothing”. In: *Proceedings of the 36th International Conference on Machine Learning*. ICML’19. PMLR, 2019. URL: <https://proceedings.mlr.press/v97/cohen19c.html>.
- [Col+17] Cody A. Coleman, Deepak Narayanan, Daniel Kang, Tian Zhao, Jian Zhang, Luigi Nardi, Peter Bailis, Kunle Olukotun, Chris Ré, and Matei Zaharia. “DAWNBench: An End-to-End Deep Learning Benchmark and Competition”. In: *Proceedings of the 2017 NeurIPS Workshop on Machine Learning Systems*. Long Beach, California, USA: Curran Associates, Inc., 2017.
- [De 11] Dean De Cock. “Ames, Iowa: Alternative to the Boston Housing Data as an End of Semester Regression Project”. In: *Journal of Statistics Education* 19.3 (2011).
- [Gu+19] Tianyu Gu, Kang Liu, Brendan Dolan-Gavitt, and Siddharth Garg. “BadNets: Evaluating Backdoor-ing Attacks on Deep Neural Networks”. In: *IEEE Access* 7 (2019), pp. 47230–47244. URL: <https://ieeexplore.ieee.org/document/8685687>.
- [HL22] Zayd Hammoudeh and Daniel Lowd. “Identifying a Training-Set Attack’s Target Using Renormalized Influence Estimation”. In: *Proceedings of the 29th ACM SIGSAC Conference on Computer and Communications Security*. CCS’22. Los Angeles, CA: Association for Computing Machinery, 2022. URL: <https://arxiv.org/abs/2201.10055>.
- [HL23] Zayd Hammoudeh and Daniel Lowd. “Reducing Certified Regression to Certified Classification for General Poisoning Attacks”. In: *Proceedings of the 1st IEEE Conference on Secure and Trustworthy Machine Learning*. SaTML’23. 2023. URL: <https://arxiv.org/abs/2208.13904>.
- [Ho98] Tin Kam Ho. “The Random Subspace Method for Constructing Decision Forests”. In: *IEEE Transactions on Pattern Analysis and Machine Intelligence* 20.8 (1998), pp. 832–844. DOI: 10.1109/34.709601.
- [Hua+20] W. Ronny Huang, Jonas Geiping, Liam Fowl, Gavin Taylor, and Tom Goldstein. “MetaPoison: Practical General-purpose Clean-label Data Poisoning”. In: *Proceedings of the 34th Conference on Neural Information Processing Systems*. NeurIPS’20. Virtual Only: Curran Associates, Inc., 2020. URL: <https://arxiv.org/abs/2004.00225>.
- [Jia+22a] Jinyuan Jia, Yupei Liu, Xiaoyu Cao, and Neil Zhenqiang Gong. “Certified Robustness of Nearest Neighbors against Data Poisoning and Backdoor Attacks”. In: *Proceedings of the 36th AAAI Conference on Artificial Intelligence*. AAAI’22. 2022. URL: <https://arxiv.org/abs/2012.03765>.
- [Jia+22b] Jinyuan Jia, Binghui Wang, Xiaoyu Cao, Hongbin Liu, and Neil Zhenqiang Gong. “Almost Tight ℓ_0 -norm Certified Robustness of Top-k Predictions against Adversarial Perturbations”. In: *Proceedings of the 10th International Conference on Learning Representations*. ICLR’22. 2022. URL: <https://openreview.net/forum?id=gJLExy3ySpu>.

- [Ke+17] Guolin Ke, Qi Meng, Thomas Finley, Taifeng Wang, Wei Chen, Weidong Ma, Qiwei Ye, and Tie-Yan Liu. “LightGBM: A Highly Efficient Gradient Boosting Decision Tree”. In: *Proceedings of the 31st International Conference on Neural Information Processing Systems*. NeurIPS’17. 2017.
- [KT06] Jon Kleinberg and Éva Tardos. *Algorithm Design*. Addison Wesley, 2006.
- [KNH14] Alex Krizhevsky, Vinod Nair, and Geoffrey Hinton. *The CIFAR-10 Dataset*. 2014.
- [Kum+20] Ram Shankar Siva Kumar, Magnus Nystrom, John Lambert, Andrew Marshall, Mario Goertzel, Andi Comissoneru, Matt Swann, and Sharon Xia. “Adversarial Machine Learning – Industry Perspectives”. In: *Proceedings of the 2020 IEEE Security and Privacy Workshops*. SPW’20. 2020. URL: <https://arxiv.org/abs/2002.05646>.
- [LeC+98] Yann LeCun, Léon Bottou, Yoshua Bengio, and Patrick Haffner. “Gradient-Based Learning Applied to Document Recognition”. In: *Proceedings of the IEEE*. Vol. 86. 1998, pp. 2278–2324.
- [LF20] Alexander Levine and Soheil Feizi. “Robustness Certificates for Sparse Adversarial Attacks by Randomized Ablation”. In: *Proceedings of the 34th AAAI Conference on Artificial Intelligence*. AAAI Press, 2020. URL: <https://arxiv.org/abs/1911.09272>.
- [LF21] Alexander Levine and Soheil Feizi. “Deep Partition Aggregation: Provable Defenses against General Poisoning Attacks”. In: *Proceedings of the 9th International Conference on Learning Representations*. ICLR’21. Virtual Only, 2021. URL: <https://arxiv.org/abs/2006.14768>.
- [LXL23] Linyi Li, Tao Xie, and Bo Li. “SoK: Certified Robustness for Deep Neural Networks”. In: *Proceedings of the 44th IEEE Symposium on Security and Privacy*. SP’23. IEEE, 2023. URL: <https://arxiv.org/abs/2009.04131>.
- [LDD21] Xiling Li, Rafael Dowsley, and Martine De Cock. “Privacy-Preserving Feature Selection with Secure Multiparty Computation”. In: *Proceedings of the 38th International Conference on Machine Learning*. ICML’21. 2021. URL: <https://arxiv.org/abs/2102.03517>.
- [Li+22] Yiming Li, Baoyuan Wu, Yong Jiang, Zhifeng Li, and Shu-Tao Xia. “Backdoor Learning: A Survey”. In: *IEEE Transactions on Neural Networks and Learning Systems* (2022). DOI: [10.1109/TNNLS.2022.3182979](https://doi.org/10.1109/TNNLS.2022.3182979). URL: <https://arxiv.org/abs/2007.08745>.
- [LCY14] Min Lin, Qiang Chen, and Shuicheng Yan. “Network in Network”. In: *Proceedings of the 2nd International Conference on Learning Representations*. ICLR’14. 2014. URL: <https://arxiv.org/abs/1312.4400>.
- [Mad+18] Aleksander Madry, Aleksandar Makelov, Ludwig Schmidt, Dimitris Tsipras, and Adrian Vladu. “Towards Deep Learning Models Resistant to Adversarial Attacks”. In: *Proceedings of the 6th International Conference on Learning Representations*. ICLR’18. 2018. URL: <https://arxiv.org/abs/1706.06083>.
- [Mal+21] Andrey Malinin, Neil Band, Yarin Gal, Mark Gales, Alexander Ganshin, German Chesnokov, Alexey Noskov, Andrey Ploskonosov, Liudmila Prokhorenkova, Ivan Provilkov, Vatsal Raina, Vyas Raina, Denis Roginskiy, Mariya Shmatova, Panagiotis Tigas, and Boris Yangel. “Shifts: A Dataset of Real Distributional Shift Across Multiple Large-Scale Tasks”. In: *Proceedings of the 35th Conference on Neural Information Processing Systems*. NeurIPS’21. Curran Associates, Inc., 2021. URL: <https://arxiv.org/abs/2107.07455>.
- [MY21] Jan Hendrik Metzen and Maksym Yatsura. “Efficient Certified Defenses Against Patch Attacks on Image Classifiers”. In: *Proceedings of the 9th International Conference on Learning Representations*. ICLR’21. 2021. URL: <https://openreview.net/forum?id=hr-3PMvDpil>.
- [Pag20] David Page. “How to Train Your ResNet”. In: (May 2020). URL: <https://myrtle.ai/learn/how-to-train-your-resnet/>.
- [Pas+19] Adam Paszke, Sam Gross, Francisco Massa, Adam Lerer, James Bradbury, Gregory Chanan, Trevor Killeen, Zeming Lin, Natalia Gimelshein, Luca Antiga, Alban Desmaison, Andreas Kopf, Edward Yang, Zachary DeVito, Martin Raison, Alykhan Tejani, Sasank Chilamkurthy, Benoit Steiner, Lu Fang, Junjie Bai, and Soumith Chintala. “PyTorch: An Imperative Style, High-Performance Deep Learning Library”. In: *Proceedings of the 33rd Conference on Neural Information Processing Systems*. NeurIPS’19. Vancouver, Canada: Curran Associates, Inc., 2019. URL: <https://arxiv.org/abs/1912.01703>.
- [Sch+19] Lukas Schott, Jonas Rauber, Matthias Bethge, and Wieland Brendel. “Towards the first adversarially robust neural network model on MNIST”. In: *Proceedings of the 7th International Conference on Learning Representations*. ICLR’19. 2019. URL: <https://openreview.net/forum?id=S1EH0sC9tX>.

- [Sha+18] Ali Shafahi, W. Ronny Huang, Mahyar Najibi, Octavian Suci, Christoph Studer, Tudor Dumitras, and Tom Goldstein. “Poison Frogs! Targeted Clean-Label Poisoning Attacks on Neural Networks”. In: *Proceedings of the 32nd Conference on Neural Information Processing Systems*. NeurIPS’18. Montreal, Canada: Curran Associates, Inc., 2018. URL: <https://arxiv.org/abs/1804.00792>.
- [SGF22] Gaurang Sriramanan, Maharshi Gor, and Soheil Feizi. “Toward Efficient Robust Training against Union of ℓ_p Threat Models”. In: *Proceedings of the 36th Conference on Neural Information Processing Systems*. NeurIPS’22. 2022. URL: <https://openreview.net/forum?id=6qdUJblMHqy>.
- [SD20] Cecilia Summers and Michael J. Dinneen. “Four Things Everyone Should Know to Improve Batch Normalization”. In: *Proceedings of the 8th International Conference on Learning Representations*. ICLR’20. Virtual Only, 2020. URL: <https://arxiv.org/abs/1906.03548>.
- [Sze+14] Christian Szegedy, Wojciech Zaremba, Ilya Sutskever, Joan Bruna, Dumitru Erhan, Ian Goodfellow, and Rob Fergus. “Intriguing Properties of Neural Networks”. In: *Proceedings of the 2nd International Conference on Learning Representations*. ICLR’14. 2014. URL: <https://arxiv.org/abs/1312.6199>.
- [TB19] Florian Tramer and Dan Boneh. “Adversarial Training and Robustness for Multiple Perturbations”. In: *Proceedings of the 33rd Conference on Neural Information Processing Systems*. NeurIPS’19. Curran Associates, Inc., 2019. URL: <https://arxiv.org/abs/1904.13000>.
- [Tra+20] Florian Tramer, Nicholas Carlini, Wieland Brendel, and Aleksander Madry. “On Adaptive Attacks to Adversarial Example Defenses”. In: *Proceedings of the 34th Conference on Neural Information Processing Systems*. NeurIPS’20. Curran Associates, Inc., 2020. URL: <https://arxiv.org/abs/2002.08347>.
- [Wal+21] Eric Wallace, Tony Z. Zhao, Shi Feng, and Sameer Singh. “Concealed Data Poisoning Attacks on NLP Models”. In: *Proceedings of the North American Chapter of the Association for Computational Linguistics*. NAACL’21. 2021. URL: <https://arxiv.org/abs/2010.12563>.
- [WLF22] Wenxiao Wang, Alexander Levine, and Soheil Feizi. “Improved Certified Defenses against Data Poisoning with (Deterministic) Finite Aggregation”. In: *Proceedings of the 39th International Conference on Machine Learning*. ICML’22. 2022. URL: <https://arxiv.org/abs/2202.02628>.
- [Web+20] Maurice Weber, Xiaojun Xu, Bojan Karlaš, Ce Zhang, and Bo Li. *RAB: Provable Robustness Against Backdoor Attacks*. 2020. arXiv: 2003.08904 [cs.LG]. URL: <https://arxiv.org/abs/2003.08904>.
- [Wei+22] Kang Wei, Jun Li, Chuan Ma, Ming Ding, Sha Wei, Fan Wu, Guihai Chen, and Thilina Ranbaduge. *Vertical Federated Learning: Challenges, Methodologies and Experiments*. 2022. arXiv: 2202.04309 [cs.LG]. URL: <https://arxiv.org/abs/2202.04309>.
- [Xia+21] Chong Xiang, Arjun Nitin Bhagoji, Vikash Sehwal, and Prateek Mittal. “PatchGuard: A Provably Robust Defense against Adversarial Patches via Small Receptive Fields and Masking”. In: *Proceedings of the 30th USENIX Security Symposium*. USENIX’21. USENIX Association, 2021.

Feature Partition Aggregation: A Fast Certified Defense Against a Union of Sparse Adversarial Attacks

Supplemental Materials

Organization of the Appendix

| | |
|---|------------|
| A Nomenclature Reference | A2 |
| B Proofs | A4 |
| B.1 Theorems and Lemma from the Main Paper | A4 |
| B.2 Lemmas from the Supplemental Materials | A6 |
| C On a Sparse Attacker that Modifies Training Labels | A8 |
| C.1 Training Instance Partitioning | A8 |
| C.2 Training Label Partitioning with Semi-Supervised Learning | A9 |
| D On Overlapping Submodel Feature Sets | A10 |
| D.1 Top 1 Certified Feature Robustness with Overlapping Feature Sets | A10 |
| D.2 Limitations of Overlapping Feature Sets | A11 |
| D.3 Empirical Evaluation of Overlapping Feature Sets for Top-1 Certified Feature Robustness | A11 |
| E Evaluation Setup | A15 |
| E.1 Hardware Setup | A15 |
| E.2 Baselines | A15 |
| E.3 Datasets | A15 |
| E.4 Network Architectures | A16 |
| E.5 Hyperparameters | A16 |
| E.6 Overview of the Certified Regression to Certified Classification Reduction | A17 |
| F Additional Experiments | A21 |
| F.1 Uncertified Accuracy | A21 |
| F.2 Detailed Experimental Results | A21 |
| F.3 Feature Partition Aggregation Model Count Hyperparameter Analysis | A31 |
| F.4 Randomized Ablation Number of Kept Features (e) Hyperparameter Analysis | A33 |
| F.5 Random vs. Deterministic Feature Partitioning | A35 |
| F.6 Model Training Times | A37 |

A Nomenclature Reference

Scalars and functions are denoted with lowercase italic letters. Vectors are denoted as lowercase bold letters. Matrices are denoted as uppercase bold letters. The j -th column of a matrix \mathbf{A} is denoted \mathbf{A}_j .

Table 2: **Nomenclature Reference:** Related symbols are grouped together. For example, the first group lists the acronyms of the methods evaluated in this work. This table includes nomenclature symbols that only appear in the supplement.

| | |
|----------------------------------|---|
| FPA | Our certified defense, feature partition aggregation, against sparse poisoning, backdoor, evasion, and patch attacks |
| RA | Randomized ablation. Certified ℓ_0 -norm defense. Proposed by Levine and Feizi [LF20] and subsequently improved by Jia et al. [Jia+22b] |
| DPA | Deep partition aggregation certified poisoning defense proposed by Levine and Feizi [LF21] |
| Patch IBP | Adversarial path defense based on interval bound propagation proposed by Chiang et al. [Chi+20b] |
| BAGCERT | Adversarial patch defense proposed by Metzzen and Yatsura [MY21] |
| LightGBM | Gradient-boosted decision tree model architecture [Ke+17] |
| r | Pointwise certified feature robustness – feature partition aggregation’s certification objective (Def. 1) |
| ρ | Pointwise ℓ_0 -norm certified evasion-only robustness (Def. 2). A weaker guarantee than certified feature robustness. |
| \tilde{r} | Pointwise certified feature and label-flipping robustness (Def. 7 – suppl. Sec. C) |
| $[m]$ | Integer set $\{1, \dots, m\}$ where $m \in \mathbb{N}$ |
| $\mathbb{1}[q]$ | Indicator function where $\mathbb{1}[q] = 1$ if q is true and 0 otherwise |
| $\ \mathbf{w}\ _0$ | ℓ_0 norm for vector \mathbf{w} , i.e., the number of non-zero elements in \mathbf{w} |
| $\mathbf{X} \ominus \mathbf{X}'$ | Set of column indices over which equal-size matrices \mathbf{X} and \mathbf{X}' differ, where $\mathbf{X} \ominus \mathbf{X}' \subseteq [d]$ |
| $\mathbf{x} \ominus \mathbf{x}'$ | Set of dimensions where vectors \mathbf{x} and \mathbf{x}' differ where $\mathbf{x} \ominus \mathbf{x}' \subseteq [d]$ |
| n | Number of training instances |
| \mathcal{X} | Feature domain where $\mathcal{X} \subseteq \mathbb{R}^d$ |
| \mathbf{x} | Feature vector where $\forall_{\mathbf{x}} \mathbf{x} \in \mathcal{X}$ |
| d | Feature dimension where $\forall_{\mathbf{x}} \mathbf{x} = d$ |
| $[d]$ | Complete feature set |
| \mathcal{Y} | Label set where $\mathcal{Y} \subseteq \mathbb{N}$ |
| y | Instance label where $\forall_y y \in \mathcal{Y}$ |
| (\mathbf{x}_i, y_i) | Arbitrary training instance where $\mathbf{x}_i \in \mathcal{X}$, $y_i \in \mathcal{Y}$, and $i \in [n]$ |
| \mathbf{X} | Training feature matrix where $\mathbf{X} := [\mathbf{x}_1 \dots \mathbf{x}_n]^\top$ and $\mathbf{X} \in \mathbb{R}^{n \times d}$ |
| \mathbf{y} | Training label vector where $\mathbf{y} := [y_1, \dots, y_n]$ |
| f | Voting-based, ensemble classifier trained over partitioned feature sets where $f : \mathcal{X} \rightarrow \mathcal{Y}$ |
| T | Number of submodels in ensemble f |
| f_t | t -th submodel in ensemble f where $t \in [T]$ and $f_t : \mathcal{X} \rightarrow \mathcal{Y}$ |
| \mathcal{S}_t | Feature subset considered by submodel f_t during training and test where $\mathcal{S}_t \subset [d]$ and $\bigsqcup_{t=1}^T \mathcal{S}_t = [d]$ |
| $\mathbf{x}_{\mathcal{S}_t}$ | Subvector of $\mathbf{x} \in \mathcal{X}$ restricted to the features subset $\mathcal{S}_t \subset [d]$ |
| D_t | Submodel f_t ’s training set |
| ϕ | Spread degree of the (overlapping) feature subsets D_1, D_2, \dots ; by default, $\phi = 1$. See suppl. Sec. D. |
| $f_t(\mathbf{x})$ | Prediction of the t -th submodel for instance $\mathbf{x} \in \mathcal{X}$ where $f_t(\mathbf{x}) \in \mathcal{Y}$ |
| $c_y(\mathbf{x})$ | Number of ensemble submodels that predict label y for feature vector \mathbf{x} where $c_y(\mathbf{x}) := \sum_{t=1}^T \mathbb{1}[f_t(\mathbf{x}) = y]$ |
| $f(\mathbf{x})$ | Top-1 model prediction for instance $\mathbf{x} \in \mathcal{X}$ where $f(\mathbf{x}) := \arg \max_{y \in \mathcal{Y}} c_y(\mathbf{x})$ |
| y_{pl} | Model plurality label where $y_{\text{pl}} := f(\mathbf{x})$ |

(Continued ...)

Table 2: **Nomenclature Reference (Continued)**: Related symbols are grouped together.

| | |
|--------------------|---|
| \ddot{y} | Label with the second most votes (i.e., the “runner up”) where $\ddot{y} := \arg \max_{y' \in \mathcal{Y}, y' \neq y} c_{y'}(\mathbf{x})$ |
| \tilde{y} | Label with the $(k + 1)$ -th most votes |
| $f(\mathbf{x}; k)$ | Top- k model prediction for instance $\mathbf{x} \in \mathcal{X}$ where $f(\mathbf{x}; k) := \arg \max_{\mathcal{Y}_k \subset \mathcal{Y}, \mathcal{Y}_k =k} \sum_{y \in \mathcal{Y}_k} c_y(\mathbf{x})$ |
| h_{tr} | Instance space mapping function where $h_{\text{tr}} : \mathcal{X} \times \mathcal{Y} \rightarrow [T]$. See suppl. Sec. C |
| $h_{\mathcal{S}}$ | Feature subset mapping function for overlapping feature sets where $h_{\mathcal{S}} : [\phi T] \rightarrow [\phi T]$. See suppl. Sec. D |
| e | Randomized ablation hyperparameter – number of kept pixels with the other $(d - e)$ ablated. |

B Proofs

This section contains all proofs for our theoretical contributions. Sec. B.1 provides the proofs for the main paper’s theoretical contributions. Due to space, some of our theoretical contributions appear only in the supplement. Sec. B.2 contains the proofs for these supplement-only theoretical contributions.

B.1 Theorems and Lemma from the Main Paper

This section provides the proofs for our theoretical contributions in the main paper.

Proof of Theorem 3

Proof. Let $\tilde{y} \in \mathcal{Y}$ denote the runner-up label where

$$\tilde{y} := \arg \max_{y' \in \mathcal{Y}, y' \neq y_{\text{pl}}} c_{y'}(\mathbf{x}). \quad (7)$$

By definition,

$$\Delta := c_{y_{\text{pl}}}(\mathbf{x}) - c_{\tilde{y}}(\mathbf{x}) \leq \forall_{y' \notin \mathcal{Y} \setminus \{y_{\text{pl}}, \tilde{y}\}} c_{y_{\text{pl}}}(\mathbf{x}) - c_{y'}(\mathbf{x}). \quad (8)$$

In words, vote-count difference Δ between plurality label y_{pl} and runner-up label \tilde{y} is smaller than the gap between y_{pl} and any other label.

In the worst case, a single feature perturbation changes a single submodel prediction $f_i(\mathbf{x})$ from plurality label y_{pl} to a label of the adversary’s choosing. Each such perturbed submodel prediction reduces the gap between the plurality label and the adversary’s chosen label by two. By Eq. (8), it takes the fewest number of vote changes for \tilde{y} to overtake plurality label y_{pl} with the proof following by induction. Δ then bounds the certified robustness. When determining r , Δ may be even or odd. We separately consider both cases below.

Case #1: Δ is odd.

Since Δ is odd, there can never be a tie between labels y_{pl} and \tilde{y} , simplifying the analysis. Then, the maximum number of submodel predictions that can change without affecting ensemble prediction $f(\mathbf{x})$ is $r \in \mathbb{N}$ satisfying

$$c_{\tilde{y}}(\mathbf{x}) + 2r < c_{y_{\text{pl}}}(\mathbf{x}) \quad (9)$$

$$r < \frac{c_{y_{\text{pl}}}(\mathbf{x}) - c_{\tilde{y}}(\mathbf{x})}{2} \quad (10)$$

$$r = \left\lfloor \frac{c_{y_{\text{pl}}}(\mathbf{x}) - c_{\tilde{y}}(\mathbf{x})}{2} \right\rfloor \quad \triangleright r \text{ must be a whole number} \quad (11)$$

$$= \left\lfloor \frac{c_{y_{\text{pl}}}(\mathbf{x}) - (c_{\tilde{y}}(\mathbf{x}) + \mathbb{1}[\tilde{y} < y_{\text{pl}}])}{2} \right\rfloor \quad \triangleright \text{Subtracting 1 has no effect when } \Delta \text{ odd} \quad (12)$$

$$= \left\lfloor \frac{c_{y_{\text{pl}}}(\mathbf{x}) - \arg \max_{y' \neq y_{\text{pl}}} (c_{y'}(\mathbf{x}) + \mathbb{1}[y' < y_{\text{pl}}])}{2} \right\rfloor \quad \triangleright \text{Eq. (7)}. \quad (13)$$

Case #2: Δ is even.

For even-valued Δ , ties can occur. If $\tilde{y} < y_{\text{pl}}$, the tie between y_{pl} and \tilde{y} is broken in favor of \tilde{y} . Then, the number of submodel predictions that can change without affecting the ensemble prediction is any $r \in \mathbb{N}$ satisfying

$$c_{\tilde{y}}(\mathbf{x}) + \mathbb{1}[\tilde{y} < y_{\text{pl}}] + 2r < c_{y_{\text{pl}}}(\mathbf{x}) \quad (14)$$

$$r \leq \frac{c_{y_{\text{pl}}}(\mathbf{x}) - (c_{\tilde{y}}(\mathbf{x}) + \mathbb{1}[\tilde{y} < y_{\text{pl}}])}{2} \quad (15)$$

$$r = \left\lfloor \frac{c_{y_{\text{pl}}}(\mathbf{x}) - (c_{\tilde{y}}(\mathbf{x}) + \mathbb{1}[\tilde{y} < y_{\text{pl}}])}{2} \right\rfloor \quad \triangleright r \text{ must be a whole number} \quad (16)$$

$$= \left\lfloor \frac{c_{y_{\text{pl}}}(\mathbf{x}) - \arg \max_{y' \neq y_{\text{pl}}} (c_{y_{\text{pl}}}(\mathbf{x}) + \mathbb{1}[y' < y_{\text{pl}}])}{2} \right\rfloor \quad \triangleright \text{Eq. (7)}. \quad (17)$$

□

Theorem 3’s definition of r follows the same basic structure as that of *deep partition aggregation* [LF21, Eq. (10)].

Proof of Theorem 4

Alg. 1’s iterative greedy strategy is formalized below.

Def. 6. Certified Feature Robustness Greedy Strategy *Given target label $y \in \mathcal{Y}$, plurality label $y_{\text{pl}} \in \mathcal{Y}$, and label $\tilde{y} \in \mathcal{Y}$ with the $(k + 1)$ -th most votes, if $c_y(\mathbf{x}) > 0$, decrement $c_y(\mathbf{x})$ by 1; otherwise, decrement $c_{y_{\text{pl}}}(\mathbf{x})$ by 1. Increment both $c_{\tilde{y}}(\mathbf{x})$ and certified feature robustness r by 1.*

Theorem 4’s proof references Def. 6 for brevity.

Proof. We follow the classic “*greedy stays ahead*” proof strategy [KT06]. In short, given some iterative greedy strategy, the greedy algorithm always does better at each iteration than any other algorithm. Also, observe that the order that the greedy strategy perturbs the labels does not affect the optimality of the bound since each perturbation is strictly increasing, additive, and fully commutative.

In short, Def. 6’s greedy strategy minimizes at each iteration the margin between y ’s vote count, $c_y(\mathbf{x})$, and the vote count of the label with the $(k + 1)$ -th most votes, i.e., $c_{\tilde{y}}(\mathbf{x})$. Recall that Theorem 3’s proof above for top-1 certified robustness only considers the runner-up label \tilde{y} since all other labels $y' \notin \mathcal{Y} \setminus \{y, \tilde{y}\}$ require at least as many label changes as runner-up \tilde{y} to overtake plurality label y . Def. 6’s greedy strategy generalizes this idea where now only the top $(k + 1)$ labels are considered and the rest of the labels ignored.

Each iteration of Alg. 1 may have a different label with the $(k + 1)$ -th most votes. For a given iteration, denote this label \tilde{y} , making label y ’s margin of remaining in the top k

$$\Delta := c_y(\mathbf{x}) - c_{\tilde{y}}(\mathbf{x}). \quad (18)$$

Trivially, maximally reducing $c_y(\mathbf{x})$ and maximally increasing $c_{\tilde{y}}(\mathbf{x})$ has the effect of maximally reducing their difference Δ . While it is always possible to increase $c_{\tilde{y}}(\mathbf{x})$, it is not always possible to always reduce $c_y(\mathbf{x})$. Our greedy approach as implemented in Alg. 1 conditions each iteration’s strategy based on whether $c_y(\mathbf{x})$ can be reduced, i.e., whether $c_y(\mathbf{x}) > 0$.

Case #1: $c_y(\mathbf{x}) > 0$.

In each iteration, a single submodel prediction is changed. Changing one submodel prediction $f_t(\mathbf{x})$ from label y to label \tilde{y} maximally decreases $c_y(\mathbf{x})$. Moreover, transferring the vote to \tilde{y} also increases $c_{\tilde{y}}(\mathbf{x})$. No other allocation of the votes could reduce Δ more in particular since the order of the votes being reallocated does not matter.

Case #2: $c_y(\mathbf{x}) = 0$.

No label can have negative votes so $c_y(\mathbf{x})$ cannot be further reduced. Reducing the margin exclusively entails maximally increasing $c_{\tilde{y}}(\mathbf{x})$. Def. 6 and Alg. 1 transfer a vote from the plurality label $y_{\text{pl}} := \arg \max_{y' \in \mathcal{Y}} c_{y'}(\mathbf{x})$ to label \tilde{y} . Transferring the vote from the plurality label guarantees that $c_{\tilde{y}}(\mathbf{x})$ monotonically increases and no vote is ever transferred twice since $k < T$. □

Proof of Lemma 5

Proof. Given T submodels and any $\mathbf{x} \in \mathcal{X}$, the most robust ensemble prediction occurs when all submodels predict $y_{\min} := \min \mathcal{Y}$,¹⁰ meaning by definition $c_{y_{\min}}(\mathbf{x}) = T$.

¹⁰Predicting y_{\min} ensures ties are broken in favor of the predicted label.

For y_{\min} to no longer be in the top- k , at least k other labels must have more votes than y_{\min} . An optimal attacker modifies the instances so each of these k labels has the same number of votes; denote this quantity as δ .

For each vote assigned to these k other labels, $c_{y_{\min}}(\mathbf{x})$ decreases by 1. To increase the vote count of k labels by δ , $c_{y_{\min}}(\mathbf{x})$ must decrease by $k\delta$. As long as $c_{y_{\min}}(\mathbf{x})$ is at least as large as the vote count for the other labels, the prediction can be certified. It follows then that

$$T - k\delta \geq \delta \tag{19}$$

$$T \geq (k + 1)\delta \tag{20}$$

$$\frac{T}{k + 1} \geq \delta . \tag{21}$$

Recall that for k labels to increase by δ votes, $c_{y_{\min}}(\mathbf{x})$ decreases by $k\delta$ meaning

$$r \leq k\delta \tag{22}$$

$$\leq \frac{kT}{k + 1} \tag{23}$$

$$\leq \left\lceil \frac{kT}{k + 1} \right\rceil . \tag{24}$$

□

B.2 Lemmas from the Supplemental Materials

This section provides the proofs for our theoretical contributions that appear only in the supplement.

Proof of Lemma 8

Proof. This proof follows directly from the proof of Thm. 3 with one difference. When training labels y_1, \dots, y_n may not be pristine, an adversary can use malicious training labels to modify a submodel prediction.

Each training label is considered by exactly one submodel. An adversarial label change has the same worst-case effect as an adversarial feature perturbation, meaning the certified robustness derivation in Thm. 3's proof applies here unchanged (other than the definition of robustness). Hence, similar to Eq. (6),

$$\tilde{r} = \left\lfloor \frac{c_y(\mathbf{x}) - \max_{y' \neq y} (c_{y'}(\mathbf{x}) + \mathbb{1}[y' < y])}{2} \right\rfloor . \tag{25}$$

□

Proof of Lemma 9

Proof. This proof follows directly from Lem. 8's proof. As above, a single adversarial label flip or feature perturbation still changes at most one submodel prediction. Training submodels with (deterministic) semi-supervised learning does not change the mechanics of the ensemble decision. Therefore, Lem. 8's certified guarantee derivation remains unchanged between partitioning the training instances versus partitioning the training labels with semi-supervised learning. □

Proof of Lemma 10

Proof. This proof follows directly from Wang et al.’s [WLF22] Theorem 2; we direct the reader to the original paper for Wang et al.’s complete derivation. For brevity, we directly apply Wang et al.’s result below.

Both FPA and Wang et al.’s deterministic finite aggregation (DFA) train an ensemble of ϕT submodels, with each submodel considering the union of ϕ disjoint sets of objects. The only difference between the two formulations is that DFA considers sets of training instances while FPA considers sets of features; the differences in the two methods’ certified guarantees arise solely out of this one difference in formulation. DFA provides guarantees w.r.t. training instances, i.e., w.r.t. overlapping objects in the sets. Since FPA’s sets instead contain feature dimensions, FPA certifies feature robustness.

Eq. (32)’s robustness bound is identical to Wang et al.’s Theorem 2, albeit with slightly different notation.

Note that Wang et al. do not contextualize their Theorem 2 w.r.t. top- k predictions. Rather Wang et al. specify their guarantees w.r.t. correct/incorrect predictions, which is equivalent to top-1 accuracy. \square

C On a Sparse Attacker that Modifies Training Labels

Sec. 2’s base formulation of feature partition aggregation trains each submodel f_i on a subset of the features $\mathcal{S}_i \subset [d]$ from all training instances. Each submodel also considers full label vector $\mathbf{y} := [y_1, \dots, y_n]$ (see Fig. 1). In the worst case, a single adversarial label flip could manipulate all T predictions, invalidating FPA’s guarantees. Whether an attacker is able to manipulate the training labels is application dependent. Previous work commonly views *clean-label attacks* (where \mathbf{y} is pristine) as the stronger threat model [Che+17; Sha+18; Hua+20; Wal+21]. To simplify the formulation and allow for a more direct comparison to existing work, we chose for our primary presentation to assume clean labels. Nonetheless, FPA’s underlying formulation can be generalized to a threat model where an adversary can modify training labels. Def. 7 formalizes a joint robustness guarantee over feature perturbations and training-label flips.

Def. 7. Certified Feature and Label-Flipping Robustness *A pointwise, deterministic guarantee $\tilde{r} \in \mathbb{N}$ w.r.t. instance (\mathbf{x}, \mathbf{y}) where for ensemble model f' trained on any training set $(\mathbf{X}', \mathbf{y}')$ and evaluated on any instance $\mathbf{x}' \in \mathcal{X}$ s.t.*

$$|\mathbf{X} \ominus \mathbf{X}' \cup \mathbf{x} \ominus \mathbf{x}'| + |\mathbf{y} \ominus \mathbf{y}'| \leq \tilde{r} \quad (26)$$

it holds that $y \in f'(\mathbf{x}'; k)$.

Similar to certified feature robustness r in Def. 1, certified feature and label robustness \tilde{r} is not w.r.t. feature values. Instead, \tilde{r} provides a stronger guarantee allowing all values – training and test – for a feature to be perturbed. Robustness \tilde{r} arbitrarily divides between feature perturbations and training-label flips.

Below we propose two extended FPA formulations, which provide certified feature and label-flipping robustness guarantees.

C.1 Training Instance Partitioning

FPA’s base formulation is particularly vulnerable to adversarial label flipping since each submodel considers full label vector \mathbf{y} . This vulnerability’s fix is very simple: partition *both* the features and training instances across the T submodels. Under this alternate formulation, a single adversarial label flip affects at most one submodel prediction, i.e., the submodel trained on that instance. Lem. 8 formalizes the top-1 certified feature and label-flipping robustness for FPA under training instance partitioning. Like Thm. 3, Lem. 8 generalizes to certify top- k predictions via Alg. 1.

Lemma 8. Top-1 Certified Robustness with Partitioned Training Instances *Given submodel feature partition $\mathcal{S}_1, \dots, \mathcal{S}_T$, where $\bigsqcup_{t=1}^T \mathcal{S}_t = [d]$, and deterministic function $h_{tr} : \mathcal{X} \times \mathcal{Y} \rightarrow [T]$ that partitions the instance space, let f be a majority voting-based ensemble of T submodels. Each deterministic submodel f_t is trained exclusively on the features in set \mathcal{S}_t as well as only those training instances (\mathbf{x}_i, y_i) where $h_{tr}(\mathbf{x}_i, y_i) = t$. For any $\mathbf{x} \in \mathcal{X}$ and $\tilde{y} \in \mathcal{Y}$, $c_{\tilde{y}}(\mathbf{x}) := |\{t \in [T] : f_t(\mathbf{x}) = \tilde{y}\}|$. Then the pointwise top-1 certified feature and label-flipping robustness of prediction $y := f(\mathbf{x})$ is*

$$\tilde{r} = \left\lfloor \frac{c_y(\mathbf{x}) - \max_{y' \neq y} (c_{y'}(\mathbf{x}) + \mathbb{1}[y' < y])}{2} \right\rfloor. \quad (27)$$

While Lem. 8’s guarantees appear *similar* to existing certified poisoning defenses such as *deep partition aggregation* (DPA) [LF21], there is a subtle yet important difference. As explained in Sec. 3, DPA’s threat model encompasses only data poisoning attacks, meaning test instance \mathbf{x} is assumed pristine. DPA does not certifiably improve the model’s robustness under backdoor or evasion attacks when \mathbf{x} is adversarially manipulated. By contrast, Lem. 8 provides certifiable robustness under sparse poisoning, backdoor, and evasion attacks – as well as adversarial label flipping. There exist backdoor attacks where Lem. 8 is provably robust but DPA is not, e.g., Gu et al.’s [Gu+19] pixel-based attacks.

Lem. 8 is no free lunch. Partitioning the training instances across the ensemble entails that each submodel is trained on even fewer data. This can degrade submodel performance. Next, we modify the above formulation to restore some of the feature information that is lost when the training instances are partitioned.

C.2 Training Label Partitioning with Semi-Supervised Learning

Sec. 2’s threat model places no constraint on the poisoning rate, i.e., the fraction of the training instances an attacker may adversarially perturb. In other words, under this threat model, perturbing a feature for one instance is equivalent, from a certification perspective, to perturbing that feature for all instances.

Under jointly partitioned features and training instances, our revised feature partition aggregation (FPA) formulation above discards significant feature information. Formally, for training instance (\mathbf{x}_i, y_i) assigned to submodel f_t (i.e., $h_{\text{tr}}(\mathbf{x}_i, y_i) = t$), features dimensions $[d] \setminus \mathcal{S}_t$ in \mathbf{x}_i are *not used in the training of any submodel*. In other words, \mathbf{x}_i ’s feature dimensions $[d] \setminus \mathcal{S}_t$ are totally ignored. Since our threat model allows a 100% poisoning rate, discarding these features does not improve the theoretical robustness.

Rethinking Sec. C.1, the primary motivation for partitioning the training instances was to ensure that a single adversarial label flip did not affect more than one submodel. To achieve that, the formulation above not only restricts each submodel’s access to some training labels, it also restricts access to the corresponding training instance’s feature information. This is heavy-handed, and a more careful partitioning is possible.

This section’s revised FPA formulation is inspired by semi-supervised learning. Each submodel f_t still considers the \mathcal{S}_t columns of matrix \mathbf{X} . The sole difference is in the training-label vector used by each submodel. Rather than partitioning the training instances like in the previous section, our semi-supervised FPA uses function h_{tr} to partition just the training *labels*. Submodel f_t treats as unlabeled any training instance (\mathbf{x}_i, y_i) where $h_{\text{tr}}(\mathbf{x}_i, y_i) \neq t$. Put simply, the only difference between the submodel training sets of our base and semi-supervised formulations lies in the training labels available to each submodel. Both formulations train each submodel on the same feature submatrix.

Lem. 9 formalizes the top-1 certified feature and label-flipping robustness (Def. 7) for FPA under training label partitioning with semi-supervised learning. Observe that Eqs. (27) and (28) define the certified feature and label-flip robustness \tilde{r} identically. Like Thm. 3 and Lem. 9 above, Lem. 9 generalizes to certify top- k predictions via Alg. 1.

Lemma 9. Top-1 Certified Robustness with Partitioned Training Labels *Given submodel feature partition $\mathcal{S}_1, \dots, \mathcal{S}_T$, where $\bigsqcup_{t=1}^T \mathcal{S}_t = [d]$, and deterministic function $h_{\text{tr}} : \mathcal{X} \times \mathcal{Y} \rightarrow [T]$ that partitions the instance space, let f be a majority voting-based ensemble of T submodels. Each deterministic submodel f_t is trained exclusively on the features in set \mathcal{S}_t as well as the training labels for those training instances (\mathbf{x}_i, y_i) where $h_{\text{tr}}(\mathbf{x}_i, y_i) = t$. For (\mathbf{x}_i, y_i) where $h_{\text{tr}}(\mathbf{x}_i, y_i) \neq t$, submodel f_t treats the instance as unlabeled. For any $\mathbf{x} \in \mathcal{X}$ and $\tilde{y} \in \mathcal{Y}$, $c_{\tilde{y}}(\mathbf{x}) := |\{t \in [T] : f_t(\mathbf{x}) = \tilde{y}\}|$. Then the pointwise top-1 certified feature and label-flipping robustness of prediction $y := f(\mathbf{x})$ is*

$$\tilde{r} = \left\lfloor \frac{c_y(\mathbf{x}) - \max_{y' \neq y} (c_{y'}(\mathbf{x}) + \mathbb{1}[y' < y])}{2} \right\rfloor. \quad (28)$$

Whether partitioning the training labels (Sec. C.2) or the training instances (Sec. C.1) yields larger certified guarantees is an empirical question, whose answer depends on the application and semi-supervised learning algorithm.

D On Overlapping Submodel Feature Sets

As Sec. 5.3 mentions, feature partition aggregation does not necessarily require that feature subsets $\mathcal{S}_1, \dots, \mathcal{S}_T$ be a partition of the full feature set $[d]$. Rather, the feature subsets can partially overlap, but the certification analysis becomes NP-hard in the general case via reduction to (partial) set cover [HL22, Lem. 11].

Recall also that deep partition aggregation (DPA) is a certified defense against poisoning attacks under a limited poisoning rate. Like FPA, DPA trains submodels on partitioned sets – specifically, partitioned training instances. Wang et al.’s [WLF22] *deterministic finite aggregation* (DFA) extends DPA where submodels are trained on *overlapping* instance sets. Just as FPA with partitioned feature sets can be viewed as the *transpose* of DPA, FPA with overlapping feature sets can be viewed as the transpose of Wang et al.’s DFA. Below we formulate FPA with overlapping feature sets as inspired by deterministic finite aggregation.

Rather than partitioning feature set $[d]$ into T subsets, consider partitioning $[d]$ into ϕT disjoint subsets where $\phi \in \mathbb{N}$. By definition, it should hold that $\phi T \leq d$. Otherwise, some subsets in the partition will be empty by the pigeonhole principle.

In our base FPA formulation, each submodel is trained on approximately $\frac{1}{T}$ -th of the features, and each feature subset is assigned to exactly one submodel. For FPA with overlapping features, each submodel is still trained on $\frac{1}{T}$ -th of the features. However, since each feature set is now $\frac{1}{\phi}$ -th the size, each overlapping submodel is assigned ϕ feature subsets. Following Wang et al. [WLF22], each feature subset is similarly assigned to ϕ submodels. Hence, ϕ is referred to as the feature subsets’ *spread degree*.

Deterministic function $h_{\mathcal{S}} : [\phi T] \rightarrow [\phi T]^{\phi}$ maps the ϕT feature subsets to the ϕT submodels. Our overlapping features empirical evaluation below defines $h_{\mathcal{S}}$ identically to Wang et al.’s h_{spread} function. Formally, let $\mathcal{T} \subset [\phi T]$ be a set drawn uniformly at random without replacement from $[\phi T]$ where $|\mathcal{T}| = \phi$. Then, the set of submodels that use feature partition $l \in [\phi T]$ is

$$h_{\mathcal{S}}(l) := \{\tau + l \bmod \phi T : \tau \in \mathcal{T}\}. \quad (29)$$

Since \mathcal{T} is constructed randomly, overlapping feature sets more closely resemble balanced random partitioning than deterministic partitioning.

There are two important differences in the analysis of FPA with partitioned versus overlapping feature sets. First, under partitioned feature sets, a single perturbed feature affects exactly one submodel. For overlapping features, each feature subset is used in the training of ϕ submodels, meaning a single perturbed feature affects ϕ submodel votes. Second, under partitioned feature sets, certification analysis exclusively considered the minimum number of models required for the runner-up label to overtake the plurality label. Under overlapping features, the runner-up label may not be the most efficient to perturb, meaning all labels must be considered in certification analysis.

The next section formalizes the top-1 certified feature robustness under overlapping feature sets.

D.1 Top 1 Certified Feature Robustness with Overlapping Feature Sets

Recall that for any $y \in \mathcal{Y}$ and $\mathbf{x} \in \mathcal{X}$,

$$c_y(\mathbf{x}) := |\{t \in [T] : f_t(\mathbf{x}) = y\}|$$

denotes the number of submodels that predict label y for \mathbf{x} . Given ϕT disjoint feature subsets where $\bigsqcup_{l=1}^{\phi T} \mathcal{S}_l = [\phi T]$, let

$$c_y(\mathbf{x}; l) := |\{t \in [T] : f_t(\mathbf{x}) = y \wedge t \in h_{\mathcal{S}}(l)\}|, \quad (30)$$

denote the number of submodels that both use feature subset \mathcal{S}_l and predict label y for \mathbf{x} . Define the multiset w.r.t. $\mathbf{x} \in \mathcal{X}$ as

$$\Delta_{(y,y')} := \{\phi + c_y(\mathbf{x}; l) - c_{y'}(\mathbf{x}; l) : l \in [\phi T]\}, \quad (31)$$

and let $\Delta_{(y,y')}^{r'}$ denote the sum of the $r' \in \mathbb{N}$ largest elements in multiset $\Delta_{(y,y')}$.

Lem. 10 defines the top-1 certified feature robustness with overlapping feature sets and fixed spread degree ϕ . Lem. 10 follows directly from Wang et al.’s [WLF22] Thm. 2.

Lemma 10. Top-1 Certified Feature Robustness with Overlapping Feature Sets and Fixed Spread Degree *Given submodel feature partition $\mathcal{S}_1, \dots, \mathcal{S}_{\phi T}$ and function $h_{\mathcal{S}}$, let f be a voting-based ensemble of ϕT submodels,*

where each deterministic submodel f_t uses the features in set

$$\bigsqcup_{\substack{l \in [\phi T] \\ t \in h_S(l)}} \mathcal{S}_l.$$

Then the pointwise top-1 certified feature robustness of prediction is $y := f(\mathbf{x})$ is $r = \min_{y' \neq y} r_{y'}$ where

$$r_{y'} := \arg \max_{r' \in \mathbb{N}} \text{s.t. } \Delta_{(y, y')}^{r'} \leq c_y(\mathbf{x}) - c_{y'}(\mathbf{x}) - \mathbb{1}[y' < y] \quad (32)$$

The next section discusses the limitations of training FPA’s submodels on overlapping feature subsets.

D.2 Limitations of Overlapping Feature Sets

Combining FPA with overlapping feature sets has two primary limitations.

First, Sec. 4.2’s top- k greedy algorithm does not apply to overlapping feature sets. Like any NP-hard problem, greedy methods may overestimate the solution necessitating an approximation factor to address any overestimation. A greedy-based, top- k certification algorithm for overlapping feature sets is left as future work.

As an alternative to Wang et al.’s [WLF22] closed-form lower bound for the certified robustness on overlapping sets of instances, Hammoudeh and Lowd [HL23] use an integer linear program to find the optimal certified robustness. In short, Hammoudeh and Lowd’s formulation trades a better certified bound for a potentially (significantly) more complex optimization. Hammoudeh and Lowd’s [HL23] linear program could be modified to determine overlapping FPA’s optimal top- k robustness.

The second major limitation of Lem. 10’s formulation is the increased computational cost versus Thm. 3’s disjoint feature sets – even without an NP-hard optimization. One of FPA’s key advantages over previous related methods like randomized ablation is FPA’s computational efficiency (Tab. 1). FPA with disjoint feature sets has computational complexity in $\mathcal{O}(T)$. In contrast, FPA as formulated in Lem. 10 with overlapping feature sets has computation complexity in $\mathcal{O}(\phi T)$. Any performance gains derived from overlapping features need to be weighed against the multiplicative increase in training and certification time.

D.3 Empirical Evaluation of Overlapping Feature Sets for Top-1 Certified Feature Robustness

This section evaluates FPA’s top-1 performance with disjoint and overlapping feature sets. The results for CIFAR10 are in Tables 3 and 4. MNIST’s results are in Tables 5, 6, and 7. Weather’s results are in Tables 8 and 9. Beyond the overlapping feature sets, the evaluation setup is identical to Sec. 6.

Recall that under overlapping features, the total number of feature partitions is ϕT . As discussed above, this quantity is functionally bounded by the dataset dimension d . For each model configuration below, we evaluate performance with spread degree ϕ set as large as possible given T without exceeding the dataset’s corresponding dimension d .

We briefly summarize these experiments’ takeaways.

Takeaway #1: *The benefits of overlapping feature sets is largest for smaller T values.* We see this trend for all three datasets. For example with CIFAR10, overlapping feature sets improved random partitioning’s performance by up to 3.5 percentage points when $T = 25$. By contrast, for CIFAR10 with $T = 115$, overlapping feature sets improved the performance by only 0.6 percentage points. We conjecture that the primary cause of this behavior is that T and the maximum spread degree are inversely related. Since feature dimension d is fixed, larger T restricts ϕ and in turn the potential benefits of overlapping feature sets.

By comparison, the spread degree of Wang et al.’s [WLF22] DFA is capped by the number of training instances. For modern datasets, the training set’s size is much larger than the feature dimension. We believe this partially explains why overlapping sets are more useful for certified poisoning defenses than FPA.

Takeaway #2: For vision datasets, deterministic partitioning generally outperforms overlapping feature sets. The trend is most visible for CIFAR10 where overlapping feature sets only marginally outperformed strided partitioning under one small case. By contrast, CIFAR10 deterministic partitioning outperformed overlapping feature sets by multiple percentage points in many cases. For MNIST, overlapping feature sets did outperform strided deterministic partitioning in particular when r is small. In many of those cases, random partitioning also performed as well as or better than strided partitioning.

Takeaway #3: Overlapping feature sets reduce the certified accuracy’s variance for random partitioning. For Weather [Mal+21], we report both the certified accuracy’s mean and standard deviation. As spread degree ϕ increased, the certified accuracy’s variance decreased by up to two-thirds. In short, overlapping feature sets mitigate the effect of poor feature partitions, which can severely degrade random partitioning’s performance.

Takeaway #4: The benefits of overlapping feature sets decrease as r increases. This trend is consistent across all three datasets over all T values. At the largest certified robustness values, overlapping feature sets can even significantly *underperform* random partitioning. We theorize the primary cause for this phenomenon is that while top-1 guarantees for disjoint feature sets are tight, Lem. 10 only lower bounds overlapping feature set’s maximum certifiable robustness. As r increases, this looseness becomes increasingly visible.

Table 3: **CIFAR10 Overlapping Feature Sets** ($T = 25$): CIFAR10 certified accuracy for our sparse defense, feature partition aggregation (FPA), with $T = 25$. “Random” denotes balanced random partitioning with disjoint submodel feature sets (i.e., spread degree $\phi = 1$). “Overlapping” denotes that the submodel feature sets were trained using Sec. D.1’s overlapping feature set formulation with the corresponding spread degree (ϕ) specified above each column. “Strided” denotes deterministic strided partitioning with disjoint submodel feature sets (Eq. (34)). The configuration with the best mean certified accuracy is shown in **bold**.

| Cert. Robust. | Random | Overlapping | | | Strided |
|---------------|--------|-------------|-------------|-------------|-------------|
| | | $\phi = 10$ | $\phi = 20$ | $\phi = 40$ | |
| 1 | 72.1 | 73.2 | 73.6 | 73.7 | 76.1 |
| 4 | 60.8 | 62.4 | 63.6 | 64.3 | 67.6 |
| 8 | 42.5 | 43.6 | 44.4 | 45.8 | 53.0 |
| 12 | 14.2 | 13.1 | 12.8 | 12.7 | 25.0 |

Table 4: **CIFAR10 Overlapping Feature Sets** ($T = 115$): CIFAR10 certified accuracy for our sparse defense, feature partition aggregation (FPA), with $T = 115$. “Random” denotes balanced random partitioning with disjoint submodel feature sets (i.e., spread degree $\phi = 1$). “Overlapping” denotes that the submodel feature sets were trained using Sec. D.1’s overlapping feature set formulation with the corresponding spread degree (ϕ) specified above each column. “Strided” denotes deterministic strided partitioning with disjoint submodel feature sets (Eq. (34)). The configuration with the best mean certified accuracy is shown in **bold**.

| Cert. Robust. | Random | Overlapping | | Strided |
|---------------|--------|-------------|-------------|-------------|
| | | $\phi = 4$ | $\phi = 8$ | |
| 1 | 61.3 | 61.5 | 61.6 | 61.2 |
| 10 | 49.6 | 49.6 | 50.2 | 51.2 |
| 20 | 36.9 | 36.8 | 37.3 | 40.0 |
| 30 | 25.1 | 24.7 | 24.8 | 29.1 |
| 40 | 14.7 | 14.1 | 14.0 | 18.9 |
| 50 | 5.7 | 5.5 | 5.4 | 8.9 |

Table 5: **MNIST Overlapping Feature Sets** ($T = 25$): MNIST certified accuracy for our sparse defense, feature partition aggregation (FPA), with $T = 25$. “Random” denotes balanced random partitioning with disjoint submodel feature sets (i.e., spread degree $\phi = 1$). “Overlapping” denotes that the submodel feature sets were trained using Sec. D.1’s overlapping feature set formulation with the corresponding spread degree (ϕ) specified above each column. “Strided” denotes deterministic strided partitioning with disjoint submodel feature sets (Eq. (34)). The configuration with the best mean certified accuracy is shown in **bold**.

| Cert. Robust. | Random | Overlapping | | | Strided |
|------------------|--------|-------------|-------------|-------------|-------------|
| | | $\phi = 10$ | $\phi = 20$ | $\phi = 30$ | |
| 1 | 93.6 | 94.7 | 94.9 | 95.0 | 94.1 |
| 4 | 84.0 | 86.5 | 87.4 | 87.6 | 86.5 |
| 8 | 57.5 | 59.9 | 60.6 | 61.8 | 66.4 |
| 12 | 11.3 | 11.5 | 10.5 | 10.8 | 20.1 |

Table 6: **MNIST Overlapping Feature Sets** ($T = 60$): MNIST certified accuracy for our sparse defense, feature partition aggregation (FPA), with $T = 60$. “Random” denotes balanced random partitioning with disjoint submodel feature sets (i.e., spread degree $\phi = 1$). “Overlapping” denotes that the submodel feature sets were trained using Sec. D.1’s overlapping feature set formulation with the corresponding spread degree (ϕ) specified above each column. “Strided” denotes deterministic strided partitioning with disjoint submodel feature sets (Eq. (34)). The configuration with the best mean certified accuracy is shown in **bold**.

| Cert. Robust. | Random | Overlapping | | Strided |
|------------------|--------|-------------|-------------|-------------|
| | | $\phi = 6$ | $\phi = 12$ | |
| 1 | 80.8 | 82.6 | 82.7 | 80.8 |
| 5 | 64.9 | 67.3 | 68.4 | 66.6 |
| 10 | 43.1 | 43.9 | 46.5 | 46.9 |
| 15 | 26.1 | 25.9 | 27.1 | 29.2 |
| 20 | 14.2 | 14.2 | 14.6 | 16.1 |
| 25 | 5.2 | 5.2 | 5.7 | 6.3 |

Table 7: **MNIST Overlapping Feature Sets** ($T = 80$): MNIST certified accuracy for our sparse defense, feature partition aggregation (FPA), with $T = 80$. “Random” denotes balanced random partitioning with disjoint submodel feature sets (i.e., spread degree $\phi = 1$). “Overlapping” denotes that the submodel feature sets were trained using Sec. D.1’s overlapping feature set formulation with the corresponding spread degree (ϕ) specified above each column. “Strided” denotes deterministic strided partitioning with disjoint submodel feature sets (Eq. (34)). The configuration with the best mean certified accuracy is shown in **bold**.

| Cert. Robust. | Random | Overlapping | | Strided |
|------------------|--------|-------------|-------------|-------------|
| | | $\phi = 6$ | $\phi = 9$ | |
| 1 | 72.2 | 73.8 | 74.5 | 68.0 |
| 8 | 46.3 | 47.2 | 48.3 | 46.2 |
| 16 | 24.0 | 24.0 | 24.5 | 25.5 |
| 24 | 12.0 | 12.1 | 12.1 | 13.2 |
| 32 | 3.1 | 2.6 | 3.2 | 5.3 |

Table 8: **Weather Overlapping Feature Sets** ($T = 11$): Certified accuracy mean and standard deviation for the Weather tabular dataset for FPA (FPA) with $T = 11$. “Random” denotes balanced random partitioning with disjoint submodel feature sets (i.e., spread degree $\phi = 1$). “Overlapping” denotes that the submodel feature sets were trained using Sec. D.1’s overlapping feature set formulation with the corresponding spread degree (ϕ) specified above each column. The configuration with the best mean certified accuracy is shown in **bold**. Results averaged over 10 trials.

| Cert. Robust. | Random | Overlapping | | | |
|------------------|----------------------------------|----------------|----------------------------------|----------------|----------------------------------|
| | | $\phi = 3$ | $\phi = 7$ | $\phi = 9$ | $\phi = 11$ |
| 1 | 78.9 \pm 1.5 | 80.1 \pm 1.1 | 79.8 \pm 0.4 | 80.1 \pm 0.4 | 80.7 \pm 0.5 |
| 2 | 70.6 \pm 2.5 | 72.6 \pm 1.9 | 73.2 \pm 0.9 | 72.1 \pm 0.7 | 73.2 \pm 0.9 |
| 3 | 58.9 \pm 3.6 | 61.2 \pm 3.0 | 61.8 \pm 1.7 | 61.7 \pm 1.1 | 61.9 \pm 1.5 |
| 4 | 42.5 \pm 4.4 | 43.7 \pm 3.8 | 40.7 \pm 2.7 | 43.9 \pm 1.5 | 44.2 \pm 1.9 |
| 5 | 19.4 \pm 4.4 | 18.2 \pm 2.9 | 17.2 \pm 2.6 | 17.3 \pm 1.5 | 17.5 \pm 1.3 |

Table 9: **Weather Overlapping Feature Sets** ($T = 31$): Certified accuracy mean and standard deviation for the Weather tabular dataset for FPA (FPA) with $T = 31$. “Random” denotes balanced random partitioning with disjoint submodel feature sets (i.e., spread degree $\phi = 1$). “Overlapping” denotes that the submodel feature sets were trained using Sec. D.1’s overlapping feature set formulation with the corresponding spread degree (ϕ) specified above each column. The configuration with the best mean certified accuracy is shown in **bold**. Results averaged over 10 trials.

| Cert. Robust. | Random | Overlapping |
|------------------|----------------------------------|----------------------------------|
| | | $\phi = 3$ |
| 1 | 61.9 \pm 1.4 | 61.0 \pm 0.9 |
| 3 | 52.7 \pm 1.4 | 53.3 \pm 0.9 |
| 6 | 36.8 \pm 1.6 | 37.6 \pm 1.0 |
| 9 | 18.3 \pm 2.4 | 17.7 \pm 1.9 |
| 12 | 3.0 \pm 1.7 | 3.1 \pm 1.1 |

E Evaluation Setup

This section details the evaluation setup used in the experiments in Sections 6, D, and F. Below, we provide our experiments’ implementation details, dataset configurations, and hyperparameter settings.

Our source code can be downloaded from <https://github.com/ZaydH/feature-partition>. All experiments were implemented and tested in Python 3.7.13. All neural networks were implemented in PyTorch version 1.11.0 [Pas+19]. LightGBM decision forests were trained using the official `lightgbm` Python module, version 3.3.3.99 [Ke+17].

E.1 Hardware Setup

Experiments were performed on a desktop system with a single AMD 5950X 16-core CPU, 64GB of 3200MHz DDR4 RAM, and a single NVIDIA 3090 GPU.

E.2 Baselines

To the extent of our knowledge, no existing method considers certified feature robustness guarantees (Def. 1). *Randomized ablation* – our most closely related method – considers ℓ_0 -norm certified robustness (Def. 2) [LF20]. RA is a specialized form of randomized smoothing [CRK19; LXL23] targeted towards sparse evasion attacks. In terms of the state of the art, Jia et al. [Jia+22b] provide the tightest certification analysis for randomized ablation – including over top- k predictions. Jia et al.’s [Jia+22b] improved version of RA serves as the primary baseline in this work.

Recall that feature partition aggregation (FPA) provides strictly stronger certified guarantees than baseline RA. Put simply, FPA is solving a harder task than baseline randomized ablation. Therefore, when FPA achieves the same certified accuracy as the baseline, FPA is performing provably better, given FPA’s stronger guarantees.

For patch robustness, we also compare FPA against certified defenses interval bound propagation [Chi+20b] and BAGCERT [MY21].

E.3 Datasets

Our empirical evaluation considers four datasets. First, MNIST [LeC+98] and CIFAR10 [KNH14] are vision classification datasets with 10 classes each.

Although all certified sparse defenses considered in this work are exclusively proposed in the context of classification, Hammoudeh and Lowd [HL23] prove that certified regression *reduces* to voting-based certified classification. Hence, it is straightforward to transform FPA and randomized ablation into certified regression defenses. We reuse this reduction and evaluate two tabular regression datasets, Weather [Mal+21] and Ames [De 11].

For Weather, we follow Hammoudeh and Lowd’s [HL23] empirical evaluation, where the objective is to predict ground temperature within $\pm 3^\circ\text{C}$ using features that include the date, time of day, longitude, and latitude. Similarly, we follow Hammoudeh and Lowd’s [HL23]’s empirical evaluation for Ames, where the objective is to predict a property’s sale price within $\pm 15\%$ of the actual price. Since ablated training requires a custom feature encoding to differentiate ablated and non-ablated features, min-max scaling was applied to both datasets’ features for RA to normalize all feature values to the range $[0, 1]$.

We chose these two regression datasets as a stand-in for vertically partitioned data, which are commonly tabular and particular vulnerable to sparse backdoor and evasion attacks.

Table 10 provides basic information about the four datasets, including their sizes and feature dimension. Table 11 provides summary statistics for the regression datasets’ test target-value (i.e., y) distribution.

Our source code automatically downloads all necessary dataset files.

Table 10: Evaluation dataset information

| Dataset | # Classes | # Feats | # Train | # Test |
|---------|-----------|---------|-----------|---------|
| CIFAR10 | 10 | 784 | 50,000 | 10,000 |
| MNIST | 10 | 1,024 | 60,000 | 10,000 |
| Weather | N/A | 128 | 3,012,917 | 531,720 |
| Ames | N/A | 352 | 2,637 | 293 |

Table 11: **Target Value Test Distribution Statistics:** Mean (\bar{y}), standard deviation (σ_y), minimum value (y_{\min}) and maximum value (y_{\max}) for the test instances’ target y value for regression datasets Weather and Ames.

| | \bar{y} | σ_y | y_{\min} | y_{\max} |
|---------|-----------|------------|------------|------------|
| Weather | 14.9°C | 10.3°C | -44.0°C | 54.0°C |
| Ames | \$184k | \$83.4k | \$12.8k | \$585k |

E.4 Network Architectures

Table 12 details the CIFAR10 neural network architecture. Specifically, we follow previous work on CIFAR10 data poisoning [HL22] and use Page’s [Pag20] ResNet9 architecture. ResNet9 is ideal for our experiments since it is very fast to train, as ranked on DAWNbench [Col+17]. ResNet9’s fast training significantly reduces the overhead of training T submodels for FPA.

We directly adapt Page’s [Pag20] published implementation¹¹ including the use of ghost batch normalization [SD20] and the CELU activation function with $\alpha = 0.075$ [Bar17].

Three forms of data augmentation were also used in line with Page’s [Pag20] implementation. First, a random crop with four pixels of padding was performed. Next, the image was flipped horizontally with a 50% probability. Finally, a random 8×8 pixel portion of the image was randomly erased. Note that these transformations were performed *after* the pixels were disabled in the image, meaning these transformations do not result in a network seeing additional pixel information.

In a separate paper, Levine and Feizi [LF21] propose *deep partition aggregation* (DPA), a certified defense against poisoning attacks. Here, we follow Levine and Feizi’s [LF21] public implementation¹² and use the Network-in-Network (NiN) architecture [LCY14] when evaluating our method on MNIST. Table 13 visualizes the MNIST NiN architecture.

E.5 Hyperparameters

For simplicity, FPA used the same hyperparameter settings for a given dataset irrespective of T . Therefore, FPA’s results could be further improved in practice by tuning the hyperparameter settings to optimize the ensemble’s performance for a specific submodel count.

Table 14 details the CIFAR10 and MNIST hyperparameter settings for feature partition aggregation.

For CIFAR10 and MNIST, we directly used Levine and Feizi’s [LF20] published randomized ablation training source code, which includes pre-specified hyperparameter settings for the learning rate, weight decay, and optimizer hyperparameters.

Recall from Sec. 6 that for the Weather and Ames datasets, FPA’s submodels are LightGBM [Ke+17] gradient-boosted decision tree (GBDT) regressors. Table 15 details FPA’s LightGBM hyperparameter settings. For a more direct comparison with randomized ablation which cannot use a GBDT, we also evaluated FPA with linear submodels. FPA’s linear submodel hyperparameter settings for the regression datasets are in Table 16.

¹¹Source code: <https://github.com/davidcpage/cifar10-fast>.

¹²Source code: <https://github.com/alevine0/DPA>.

Table 12: ResNet9 neural network architecture

| | | | | | |
|---------|-------------|---------|---------|--------------|-------|
| | Conv1 | In=3 | Out=64 | Kernel=3 × 3 | Pad=1 |
| | BatchNorm2D | Out=64 | | | |
| | CELU | | | | |
| | Conv2 | In=64 | Out=128 | Kernel=3 × 3 | Pad=1 |
| | BatchNorm2D | Out=128 | | | |
| | CELU | | | | |
| | MaxPool2D | 2 × 2 | | | |
| ResNet1 | ConvA | In=128 | Out=128 | Kernel=3 × 3 | Pad=1 |
| | BatchNorm2D | Out=128 | | | |
| | CELU | | | | |
| | ConvB | In=128 | Out=128 | Kernel=3 × 3 | Pad=1 |
| | BatchNorm2D | Out=128 | | | |
| | CELU | | | | |
| | Conv3 | In=128 | Out=256 | Kernel=3 × 3 | Pad=1 |
| | BatchNorm2D | Out=256 | | | |
| | CELU | | | | |
| | MaxPool2D | 2 × 2 | | | |
| | Conv4 | In=256 | Out=512 | Kernel=3 × 3 | Pad=1 |
| | BatchNorm2D | Out=512 | | | |
| | CELU | | | | |
| | MaxPool2D | 2 × 2 | | | |
| ResNet2 | ConvA | In=512 | Out=512 | Kernel=3 × 3 | Pad=1 |
| | BatchNorm2D | Out=512 | | | |
| | CELU | | | | |
| | ConvB | In=512 | Out=512 | Kernel=3 × 3 | Pad=1 |
| | BatchNorm2D | Out=512 | | | |
| | CELU | | | | |
| | MaxPool2D | 4 × 4 | | | |
| | Linear | Out=10 | | | |

Levine and Feizi [LF20] only evaluate classification datasets in their original paper. As such, there are no existing hyperparameter settings for randomized ablation on Weather and Ames. We manually tuned randomized ablation’s learning rate for the regression datasets considering all values in the set $\{10^{-2}, 10^{-3}, 10^{-4}\}$. We also tested numerous different settings for the number of training epochs. To ensure a strong baseline, we report the best performing randomized ablation hyperparameter settings.

Recall from Sec. 3 that randomized ablation only provides probabilistic guarantees. By contrast, feature partition aggregation provides deterministic guarantees. To facilitate a more direct comparison between certified feature and ℓ_0 -norm guarantees, $\alpha = 0.0001$ in all experiments.

E.6 Overview of the Certified Regression to Certified Classification Reduction

Hammoudeh and Lowd [HL23] provide a reduction from certified regression to (voting-based) certified classification. Hammoudeh and Lowd [HL23] frame this reduction primarily in the context of poisoning attacks, but the reduction generalizes to other voting-based certified classifiers. For full details on the reduction from certified regression to

certified classification, we direct the reader to Hammoudeh and Lowd’s [HL23] original paper. We briefly summarize the reduction below.

Consider a multiset of real-valued “votes” $\mathcal{V} \in \mathbb{R}^T$, where Hammoudeh and Lowd [HL23] assume for simplicity that T is odd. These “votes” could be generated from an ensemble of independent submodels in the case of deep partition aggregation [LF21] and FPA. These votes could also be generated from a smoothing-based classifier such as randomized ablation. Regardless, for voting-based real-valued regression, model f ’s decision function for arbitrary instance $\mathbf{x} \in \mathcal{X}$ is

$$f(\mathbf{x}) := \text{med } \mathcal{V}, \tag{33}$$

where med denotes the median operator.

Let $y \in \mathbb{R}$ denote the true *target* value for \mathbf{x} and let $\xi_l, \xi_u \in \mathbb{R}_{\geq 0}$ be arbitrary non-negative constants. Hammoudeh and Lowd’s [HL23] formulation seeks to certify the pointwise robustness of $\xi_l \leq f(\mathbf{x}) \leq \xi_u$.¹³ Below, we discuss certifying a one-sided upper bound $f(\mathbf{x}) \leq \xi_u$. As Hammoudeh and Lowd [HL23] explain, certifying a two-sided bound is equivalent to taking the minimum robustness of the one-sided lower and upper bounds.

Consider binarizing multiset \mathcal{V} as $\mathcal{V}_{\pm 1} := \{\text{sgn}(v - \xi_u) : v \in \mathcal{V}\}$, where $\text{sgn}(\cdot)$ is the signum function. Intuitively, our goal is to transform each real-valued instance in the multiset into a binary label, either -1 or $+1$. Certified defenses such as deep partition aggregation [LF20], our sparse defense feature partition aggregation (FPA), and randomized ablation (RA) turn a multiset of votes into certified guarantees. Hammoudeh and Lowd’s [HL23] key insight is that the median and plurality labels of a binary multiset (e.g., $\mathcal{V}_{\pm 1}$) with odd-valued cardinality are always equal. In short, certifying when a multiset’s median exceeds some threshold (e.g., ξ_u) is equivalent to certifying the perturbation of the plurality label of binarized multiset $\mathcal{V}_{\pm 1}$ [HL23, Lem 6]. Hammoudeh and Lowd’s [HL23] reduction allows us to change the underlying prediction mechanism from a classifier to a regressor and directly reuse a voting-based certified classifier’s robustness certification mechanism.

Hence, while our feature partition aggregation (FPA) and baseline randomized ablation are formulated as certified classifiers, both can be reformulated as certified regressors using the reduction of Hammoudeh and Lowd [HL23]. In practice, the primary change made to both defenses is that the underlying learner(s) predict a real value instead of a label.

Since regression has no concept of a top- k accuracy, this reduction is specific to top-1 predictions. For regression, certified accuracy denotes that the model prediction satisfies $\xi_l \leq f(\mathbf{x}) \leq \xi_u$, even after r feature perturbations.

For smoothing-based methods like randomized ablation, the reduction of Hammoudeh and Lowd [HL23] is functionally very similar to Chiang et al.’s [Chi+20a] *median smoothing*. The two methods have slightly different formulations depending on the specification of the bounds.

¹³We use the exact same definitions for ξ_l and ξ_u as Hammoudeh and Lowd [HL23]. Specifically for the Weather dataset, our experiments used $\xi_l = y - 3^\circ\text{C}$ and $\xi_u = y + 3^\circ\text{C}$. For the Ames dataset, our experiments used $\xi_l = y - 15\%y$ and $\xi_u = y + 15\%y$.

Table 13: Network-in-Network neural network architecture

| | | | | | |
|-----------------|-------------|---------|---------|--------------|-------|
| Block 1 | Conv1 | In=3 | Out=192 | Kernel=5 × 5 | Pad=2 |
| | BatchNorm2D | Out=192 | | | |
| | ReLU | | | | |
| | Conv2 | In=192 | Out=160 | Kernel=1 × 1 | Pad=1 |
| | BatchNorm2D | Out=160 | | | |
| | ReLU | | | | |
| | Conv3 | In=160 | Out=96 | Kernel=1 × 1 | Pad=1 |
| | BatchNorm2D | Out=96 | | | |
| | ReLU | | | | |
| MaxPool2D | 3 × 3 | | | | |
| Block 2 | Conv1 | In=96 | Out=192 | Kernel=5 × 5 | Pad=2 |
| | BatchNorm2D | Out=192 | | | |
| | ReLU | | | | |
| | Conv2 | In=192 | Out=192 | Kernel=1 × 1 | Pad=1 |
| | BatchNorm2D | Out=192 | | | |
| | ReLU | | | | |
| | Conv3 | In=192 | Out=192 | Kernel=1 × 1 | Pad=1 |
| | BatchNorm2D | Out=192 | | | |
| | ReLU | | | | |
| AvgPool2D | 3 × 3 | | | | |
| Block 3 | Conv1 | In=192 | Out=192 | Kernel=3 × 3 | Pad=1 |
| | BatchNorm2D | Out=192 | | | |
| | ReLU | | | | |
| | Conv2 | In=192 | Out=192 | Kernel=1 × 1 | Pad=1 |
| | BatchNorm2D | Out=192 | | | |
| | ReLU | | | | |
| | Conv3 | In=192 | Out=192 | Kernel=1 × 1 | Pad=1 |
| | BatchNorm2D | Out=192 | | | |
| | ReLU | | | | |
| GlobalAvgPool2D | Out=192 | | | | |
| Linear | Out=10 | | | | |

Table 14: FPA’s neural network training hyperparameters

| | CIFAR10 | MNIST |
|-------------------------|-------------------|----------------------|
| Data Augmentation? | ✓ | |
| Validation Split | N/A | 5% |
| Optimizer | SGD | AdamW |
| Batch Size | 512 | 128 |
| # Epochs | 80 | 25 |
| Learning Rate (Peak) | $1 \cdot 10^{-3}$ | $3.16 \cdot 10^{-4}$ |
| Learning Rate Scheduler | One cycle | Cosine |
| Weight Decay (L_2) | $1 \cdot 10^{-1}$ | $1 \cdot 10^{-3}$ |

Table 15: Regression datasets LightGBM submodel training hyperparameters

| | Weather | Ames |
|-------------------|---------|------|
| Boosting Type | GBDT | GBDT |
| # Estimators | 500 | 500 |
| Max. Depth | 10 | 5 |
| Max. # Leaves | 127 | 32 |
| L_2 Regularizer | 0 | 0 |
| Objective | Huber | MAE |
| Learning Rate | 0.5 | 0.3 |
| Subsampling | 0.9 | 0.2 |

Table 16: Regression datasets linear submodel training hyperparameters

| | Weather | Ames |
|-------------------|----------------------|----------------------|
| L_1 Regularizer | $3.16 \cdot 10^{-3}$ | $4.15 \cdot 10^{-5}$ |
| Max. # Iterations | $1 \cdot 10^7$ | $1 \cdot 10^6$ |
| Tolerance | $1 \cdot 10^{-8}$ | $1 \cdot 10^{-8}$ |

F Additional Experiments

The limited space prevents us from including all experimental results in the main paper. We provide additional results below.

F.1 Uncertified Accuracy

Table 17 provides the uncertified accuracy when training a single model ($T = 1$) on each of Sec. 6’s four datasets. Uncertified accuracy means that the models are *completely non-robust*. Nonetheless, the uncertified accuracy provides an upper-bound reference for the maximum achievable accuracy given the training set and the model architectures we used.

For regression, the “uncertified accuracy” denotes the single model’s prediction satisfies the error bounds, i.e., $\xi_l \leq f(\mathbf{x}) \leq \xi_u$. Given arbitrary instance (\mathbf{x}, y) , we follow Hammoudeh and Lowd [HL23] and use $\xi_l = y - 3^\circ\text{C}$ and $\xi_u = y + 3^\circ\text{C}$ for Weather. We also follow Hammoudeh and Lowd [HL23] and use $\xi_l = y - 15\%y$ and $\xi_u = y + 15\%y$ for Ames.

Table 17: **Uncertified Accuracy:** Prediction accuracy when training a single model on all model features, i.e., $T = 1$. These values represent an upper bound on the potential accuracy of our method given the training set, model architecture, and hyperparameters.

| Dataset | Accuracy | | |
|---------|----------|--------|--------|
| | Top 1 | Top 2 | Top 3 |
| CIFAR10 | 95.40% | 95.86% | 96.10% |
| MNIST | 99.57% | 99.57% | 99.62% |
| Weather | 92.61% | N/A | N/A |
| Ames | 81.91% | N/A | N/A |

F.2 Detailed Experimental Results

Due to space, Sec. 6 contains only summarized graphical results. This section provides our detailed results including separately plotting results for the two randomized ablation hyperparameter settings – larger e with higher accuracy but lower robustness and smaller e with lower accuracy but higher robustness. This section also includes summarized numerical results across multiple certified feature robustness values.

Detailed results for the four datasets are separated into different subsections. Classification datasets CIFAR10 and MNIST are Secs. F.2.1 and F.2.2, respectively. Regression datasets Weather and Ames are in Secs. F.2.3 and F.2.4, respectively.

For datasets that used deterministic feature partitioning (e.g., CIFAR10 and MNIST), the certified accuracy variance is very low ($<0.2\%$ for a given r). As such, this section provides only mean results.

F.2.1 CIFAR10

This section provides the complete detailed results for CIFAR10 [KNH14]. These results are visualized in Fig. 2 in the main paper as a single combined figure. The broken-out results are shown in graphical form in Fig. 4 and numerical form in Tables 18 and 19.

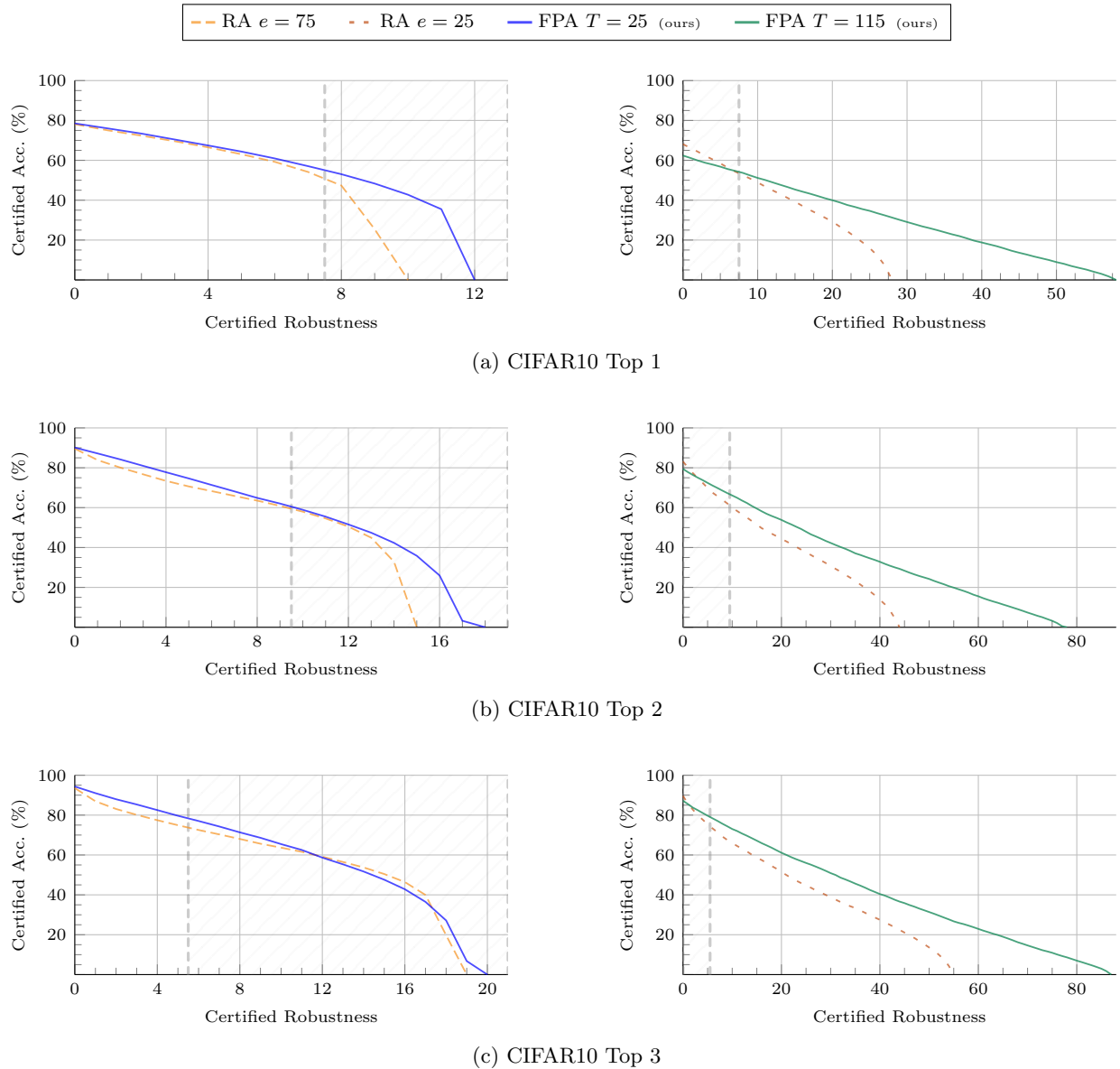


Figure 4: **CIFAR10 Certified Accuracy Detailed Results:** Certified accuracy for the CIFAR10 dataset with feature partition aggregation (FPA) and baseline randomized ablation (RA). Figure 2 in the main paper combined the results for two hyperparameter settings: higher accuracy, lower robustness as well as lower accuracy, higher robustness. These two hyperparameter settings in Fig. 2 were separated by a gray line (\cdots). Here those results are broken out into two separate plots, with the excluded region in Fig. 2 marked with gray diagonal lines. The corresponding numerical results are in Tables 18 and 19.

Table 18: **CIFAR10 Certified Accuracy for $e = 75$** : Certified accuracy (%) for the CIFAR10 dataset with randomized ablation’s (RA) number of kept pixels $e = 75$. These results correspond to Figure 2 in the main paper and Figure 4 in the supplement. For each certified robustness value, the method with the largest certified accuracy is shown in **bold**.

| | Cert. Robust. | Rand. Ablate $e = 75$ | FPA $T = 25$ |
|-------|------------------|--------------------------|-----------------|
| Top 1 | 1 | 75.0 | 76.0 |
| | 5 | 63.0 | 64.4 |
| | 10 | 0.0 | 42.7 |
| Top 2 | 1 | 83.9 | 87.2 |
| | 5 | 70.6 | 74.7 |
| | 10 | 58.0 | 58.9 |
| | 15 | 0.0 | 35.9 |
| Top 3 | 1 | 87.0 | 91.0 |
| | 5 | 74.9 | 79.7 |
| | 10 | 63.7 | 65.5 |
| | 15 | 50.5 | 47.6 |

Table 19: **CIFAR10 Certified Accuracy for $e = 25$** : Certified accuracy (%) for the CIFAR10 dataset with randomized ablation’s (RA) number of kept pixels $e = 25$. These results correspond to Figure 2 in the main paper and Figure 4 in the supplement. For each certified robustness value, the method with the largest certified accuracy is shown in **bold**.

| | Cert. Robust. | Rand. Ablate | FPA |
|-------|------------------|--------------|-------------|
| | | $e = 25$ | $T = 115$ |
| Top 1 | 1 | 66.2 | 61.2 |
| | 10 | 48.9 | 51.2 |
| | 20 | 29.2 | 40.0 |
| | 30 | 0.0 | 29.1 |
| | 40 | 0.0 | 18.8 |
| | 50 | 0.0 | 8.9 |
| Top 2 | 1 | 80.2 | 77.8 |
| | 10 | 60.1 | 66.1 |
| | 20 | 44.4 | 53.9 |
| | 30 | 30.9 | 42.3 |
| | 40 | 13.8 | 32.8 |
| | 50 | 0.0 | 24.2 |
| | 60 | 0.0 | 15.5 |
| 70 | 0.0 | 7.4 | |
| Top 3 | 1 | 85.9 | 85.6 |
| | 10 | 66.0 | 73.0 |
| | 20 | 51.5 | 61.1 |
| | 30 | 38.7 | 50.9 |
| | 40 | 27.5 | 40.4 |
| | 50 | 13.6 | 31.4 |
| | 60 | 0.0 | 22.9 |
| | 70 | 0.0 | 14.6 |
| 80 | 0.0 | 7.0 | |

F.2.2 MNIST

This section provides the complete detailed results for MNIST [LeC+98]. These results are visualized in Fig. 2 in the main paper as a single combined figure. The broken-out results are shown in graphical form in Fig. 5 and numerical form in Tables 20 and 21.

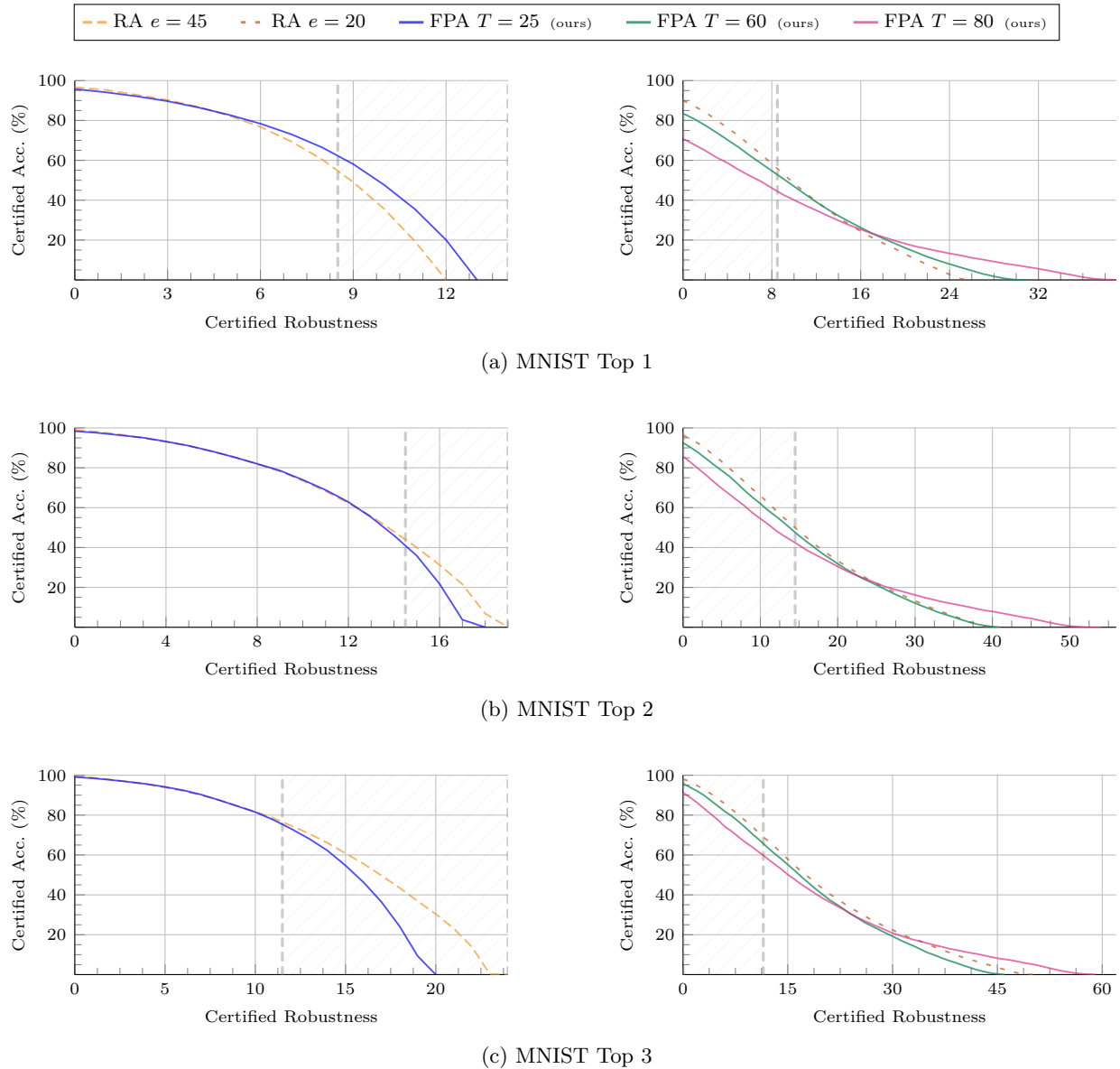


Figure 5: **MNIST Certified Accuracy Detailed Results:** Certified accuracy for the MNIST dataset with feature partition aggregation (FPA) and baseline randomized ablation (RA). Figure 2 in the main paper combined the results for two hyperparameter settings: higher accuracy, lower robustness as well as lower accuracy, higher robustness. These two hyperparameter settings in Fig. 2 were separated by a gray line (\cdots). Here those results are broken out into two separate plots, with the excluded region in Fig. 2 marked with gray diagonal lines. The corresponding numerical results are in Tables 20 and 21.

Table 20: **MNIST Certified Accuracy for $e = 45$** : Certified accuracy (%) for the MNIST dataset with randomized ablation’s (RA) number of kept pixels $e = 45$. These results correspond to Figure 2 in the main paper and Figure 5 in the supplement. For each certified robustness value, the method with the largest certified accuracy is shown in **bold**.

| | Cert. Robust. | Rand. Ablate | FPA |
|-------|------------------|--------------|-------------|
| | | $e = 45$ | $T = 25$ |
| Top 1 | 1 | 95.3 | 94.1 |
| | 5 | 82.3 | 82.8 |
| | 10 | 35.6 | 47.7 |
| Top 2 | 1 | 98.0 | 97.5 |
| | 5 | 90.9 | 91.0 |
| | 10 | 73.5 | 74.0 |
| | 15 | 40.0 | 35.9 |
| Top 3 | 1 | 98.8 | 98.5 |
| | 5 | 93.8 | 94.2 |
| | 10 | 81.7 | 81.5 |
| | 15 | 60.8 | 54.7 |

Table 21: **MNIST Certified Accuracy for $e = 20$** : Certified accuracy (%) for the MNIST dataset with randomized ablation’s (RA) number of kept pixels $e = 20$. These results correspond to Figure 2 in the main paper and Figure 5 in the supplement. For each certified robustness value, the method with the largest certified accuracy is shown in **bold**.

| | Cert. Robust. | Rand. Ablate | FPA | |
|-------|------------------|--------------|-------------|-------------|
| | | $e = 20$ | $T = 60$ | $T = 80$ |
| Top 1 | 1 | 87.2 | 80.8 | 67.9 |
| | 8 | 58.3 | 54.7 | 46.1 |
| | 16 | 24.4 | 26.3 | 25.4 |
| | 24 | 2.7 | 8.0 | 13.3 |
| | 32 | 0.0 | 0.0 | 5.6 |
| Top 2 | 1 | 94.5 | 90.2 | 82.7 |
| | 10 | 66.0 | 62.0 | 54.5 |
| | 20 | 33.3 | 31.8 | 30.5 |
| | 30 | 13.2 | 12.1 | 16.2 |
| | 40 | 0.0 | 0.3 | 7.9 |
| Top 3 | 0 | 98.1 | 95.9 | 91.3 |
| | 10 | 74.0 | 70.3 | 63.8 |
| | 20 | 43.1 | 40.2 | 38.3 |
| | 30 | 22.4 | 19.2 | 20.8 |
| | 40 | 8.7 | 4.7 | 11.7 |
| | 50 | 0.0 | 0.0 | 5.2 |

F.2.3 Weather

This section provides the complete detailed results for Malinin et al.’s [Mal+21] Weather regression dataset. The results are visualized in Fig. 3 in the main paper as a single combined figure. The broken-out results are shown in graphical form in Fig. 6 and numerical form in Tables 22 and 23. Recall that while FPA can use any submodel architecture, randomized ablation is limited to using model architectures that are stochastically trained. For Weather, gradient-boosted decision trees (e.g., LightGBM) outperform linear models. However, RA cannot use GBDTs and instead uses a linear model (in line with Hammoudeh and Lowd’s [HL23] original evaluation of Weather). For a more direct comparison with the baseline, we report FPA’s performance using both LightGBM GBDTs and linear submodels.

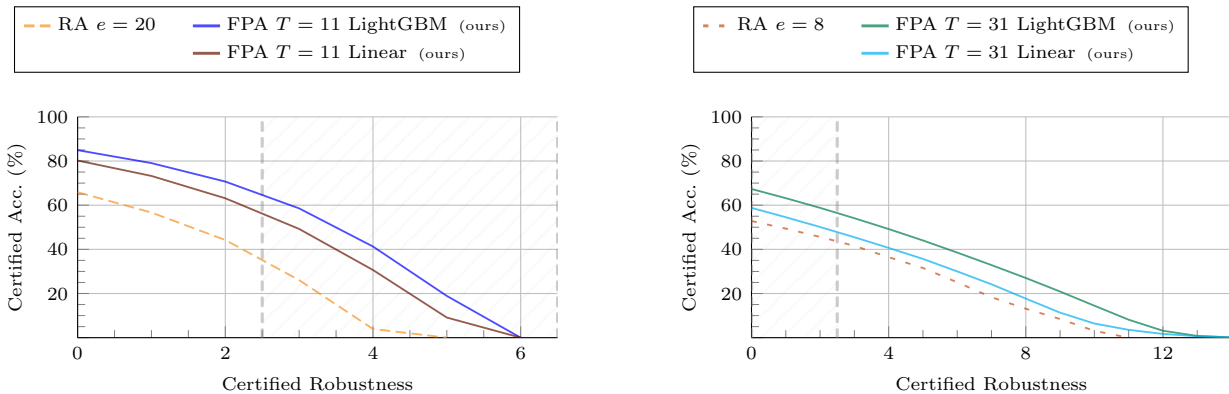


Figure 6: **Weather Certified Accuracy Detailed Results:** Certified accuracy for the Weather dataset with feature partition aggregation (FPA) and baseline randomized ablation (RA). Figure 3 in the main paper combined the results for two hyperparameter settings: higher accuracy, lower robustness as well as lower accuracy, higher robustness. These two hyperparameter settings in Fig. 3 were separated by a gray line (---). Here those results are broken out into two separate plots, with the excluded region in Fig. 3 marked with gray diagonal lines. The corresponding numerical results are in Tables 22 and 23.

Table 22: **Weather Certified Accuracy for $e = 20$:** Certified accuracy (%) for the Weather dataset with randomized ablation’s (RA) number of kept pixels $e = 20$. These results correspond to Figure 3 in the main paper and Figure 6 in the supplement. For each certified robustness value, the method with the largest certified accuracy is shown in **bold**.

| Cert. Robust. | Rand. Ablate | FPA ($T = 11$) | |
|---------------|--------------|------------------|--------|
| | $e = 20$ | LightGBM | Linear |
| 1 | 56.7 | 79.1 | 73.2 |
| 2 | 44.2 | 70.7 | 63.1 |
| 3 | 26.1 | 58.6 | 49.2 |
| 4 | 3.9 | 41.3 | 30.6 |
| 5 | 0.0 | 18.9 | 9.1 |

Table 23: **Weather Certified Accuracy for $e = 8$** : Certified accuracy (%) for the Weather dataset with randomized ablation’s (RA) number of kept pixels $e = 8$. These results correspond to Figure 3 in the main paper and Figure 6 in the supplement. For each certified robustness value, the method with the largest certified accuracy is shown in **bold**.

| Cert. Robust. | Rand. Ablate | FPA ($T = 31$) | |
|------------------|--------------|------------------|--------|
| | $e = 8$ | LightGBM | Linear |
| 1 | 49.4 | 63.2 | 54.5 |
| 3 | 41.6 | 54.1 | 45.5 |
| 6 | 25.1 | 38.5 | 30.0 |
| 9 | 8.4 | 20.9 | 11.3 |
| 12 | 0.0 | 3.1 | 1.7 |

F.2.4 Ames

This section provides the complete detailed results for De Cock’s [De 11] Ames regression dataset. The results are visualized in Fig. 3 in the main paper as a single combined figure. The broken-out results are shown in graphical form in Fig. 7 and numerical form in Tables 24 and 25.

Recall that while FPA can use any submodel architecture, randomized ablation is limited to using model architectures that are stochastically trained. For Ames, gradient-boosted decision trees (e.g., LightGBM) generally outperform linear models. However, RA cannot use GBDTs and instead uses a linear model. For a more direct comparison with the baseline, we report FPA’s performance using both LightGBM GBDTs and linear submodels.

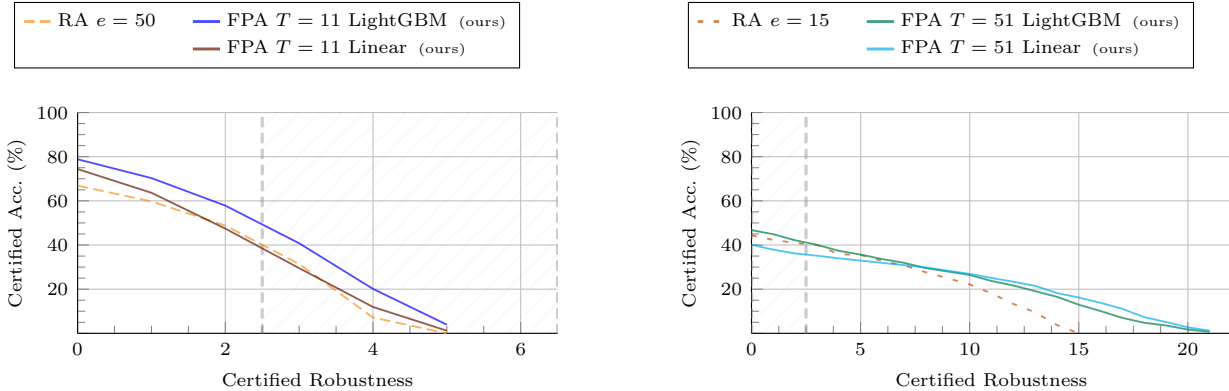


Figure 7: **Ames Certified Accuracy Detailed Results:** Certified accuracy for the Ames dataset with feature partition aggregation (FPA) and baseline randomized ablation (RA). Figure 3 in the main paper combined the results for two hyperparameter settings: higher accuracy, lower robustness as well as lower accuracy, higher robustness. These two hyperparameter settings in Fig. 3 were separated by a gray line (---). Here those results are broken out into two separate plots, with the excluded region in Fig. 3 marked with gray diagonal lines. The corresponding numerical results are in Tables 24 and 25.

Table 24: **Ames Certified Accuracy for $e = 50$:** Certified accuracy (%) for the Ames dataset with randomized ablation’s (RA) number of kept pixels $e = 50$. These results correspond to Figure 3 in the main paper and Figure 7 in the supplement. For each certified robustness value, the method with the largest certified accuracy is shown in **bold**.

| Cert. Robust. | Rand. Ablate | FPA ($T = 11$) | |
|---------------|--------------|------------------|--------|
| | $e = 50$ | LightGBM | Linear |
| 1 | 59.7 | 70.3 | 63.7 |
| 2 | 48.8 | 57.9 | 47.4 |
| 3 | 31.4 | 40.8 | 29.5 |
| 4 | 7.2 | 20.1 | 11.9 |
| 5 | 0.0 | 3.9 | 1.2 |

Table 25: **Ames Certified Accuracy for $e = 15$** : Certified accuracy (%) for the Ames dataset with randomized ablation’s (RA) number of kept pixels $e = 15$. These results correspond to Figure 3 in the main paper and Figure 7 in the supplement. For each certified robustness value, the method with the largest certified accuracy is shown in **bold**.

| Cert. Robust. | Rand. Ablate | FPA ($T = 51$) | |
|------------------|--------------|------------------|-------------|
| | $e = 15$ | LightGBM | Linear |
| 1 | 42.3 | 44.9 | 37.9 |
| 5 | 35.5 | 35.7 | 32.9 |
| 10 | 22.2 | 26.5 | 27.0 |
| 15 | 0.0 | 13.0 | 16.2 |
| 20 | 0.0 | 1.7 | 2.7 |

F.3 Feature Partition Aggregation Model Count Hyperparameter Analysis

For each dataset in Sec. 6, we report results for two or three submodel counts T . This section more directly explores how T affects the performance of feature partition aggregation – both in terms of the certified accuracy as well as the maximum certified robustness. Fig. 8 reports the performance of FPA for multiple T values for all four datasets in Sec. 6. Fig. 8 also visualizes each dataset’s uncertified accuracy (.....), where a single model is trained on all features. Sec. 6.1’s “better peak robustness” T hyperparameter setting for each dataset is visualized as

These experiments used the same evaluation setup as Sec. 6’s main experiments. For classification datasets CIFAR10 [KNH14] and MNIST [LeC+98], results for top-1 and top-3 predictions are provided. For regression datasets Weather [Mal+21] and Ames [De 11], results are provided for both LightGBM [Ke+17] and linear submodels.

The exact effect of T differs by dataset. As a general rule, increasing T decreases the ensemble’s peak accuracy (although not necessarily monotonically in the case of deterministic partitioning). Recall that Lem. 5 proves the relationship between T and the maximum top- k certified robustness. Fig. 8 visualizes this relationship where increasing T generally increases the maximum certified robustness.

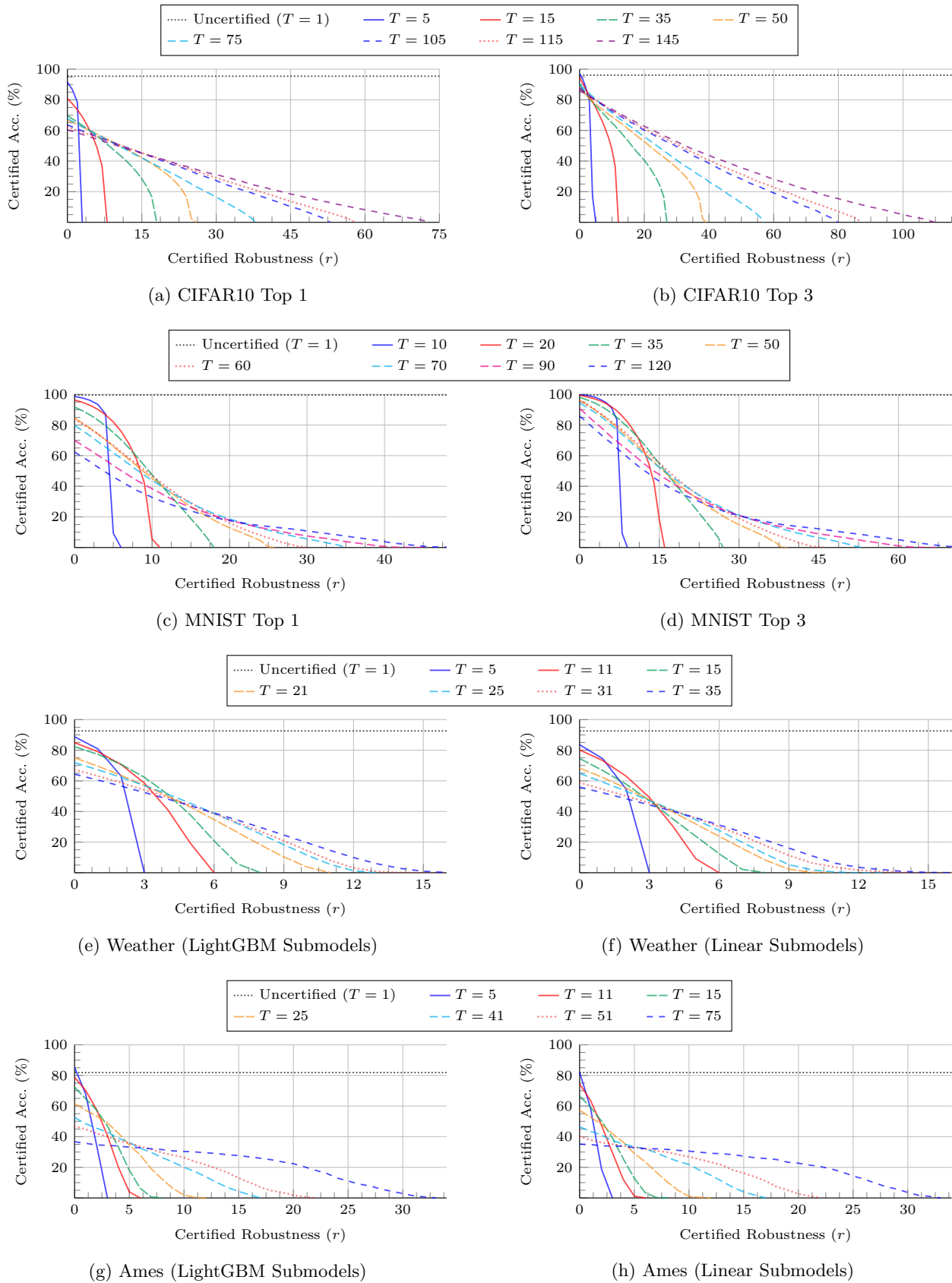


Figure 8: **Effect of Submodel Count T on Certified Feature Robustness:** Mean certified accuracy for our sparse defense, feature partition aggregation, across different submodel counts (T). Uncertified accuracy (.....) visualizes the peak accuracy of a single model ($T = 1$) trained on all features; these single model predictions are completely non-robust and provided only for reference. For all three datasets, increasing T decreases peak accuracy (when $r = 0$) but increases the maximum certifiable robustness (Lem. 5). Each T is generally optimal (i.e., achieves the largest certified accuracy) for a specific certified robustness range.

F.4 Randomized Ablation Number of Kept Features (e) Hyperparameter Analysis

As discussed in Secs. 3 and 6, ℓ_0 -norm certified defense randomized ablation (RA) is based on randomized smoothing where predictions are averaged across multiple randomly perturbed inputs. For each input, $e \in \mathbb{N}$ features in $\mathbf{x} \in \mathcal{X}$ are randomly selected to be kept at their original value, and the rest of the features are ablated, i.e., marked as unused. In short, e controls RA’s accuracy versus robustness tradeoff where larger e increases the classifier’s accuracy at the expense of a smaller maximum achievable robustness (ρ). By contrast, a small e decreases the model’s accuracy but increases the maximum achievable certified robustness.

In Sec. 6, we compare the performance of baseline RA against feature partition aggregation for two values of e – one that is higher accuracy but lower robustness and the other with lower accuracy but higher robustness. Fig. 9 provides results for RA’s performance for additional values of e for all four datasets in Sec. 6, namely CIFAR10 [KNH14], MNIST [LeC+98], Weather [Mal+21], and Ames [De 11]. Fig. 9 also visualizes each dataset’s uncertified accuracy (.....), where a single model is trained on all features.

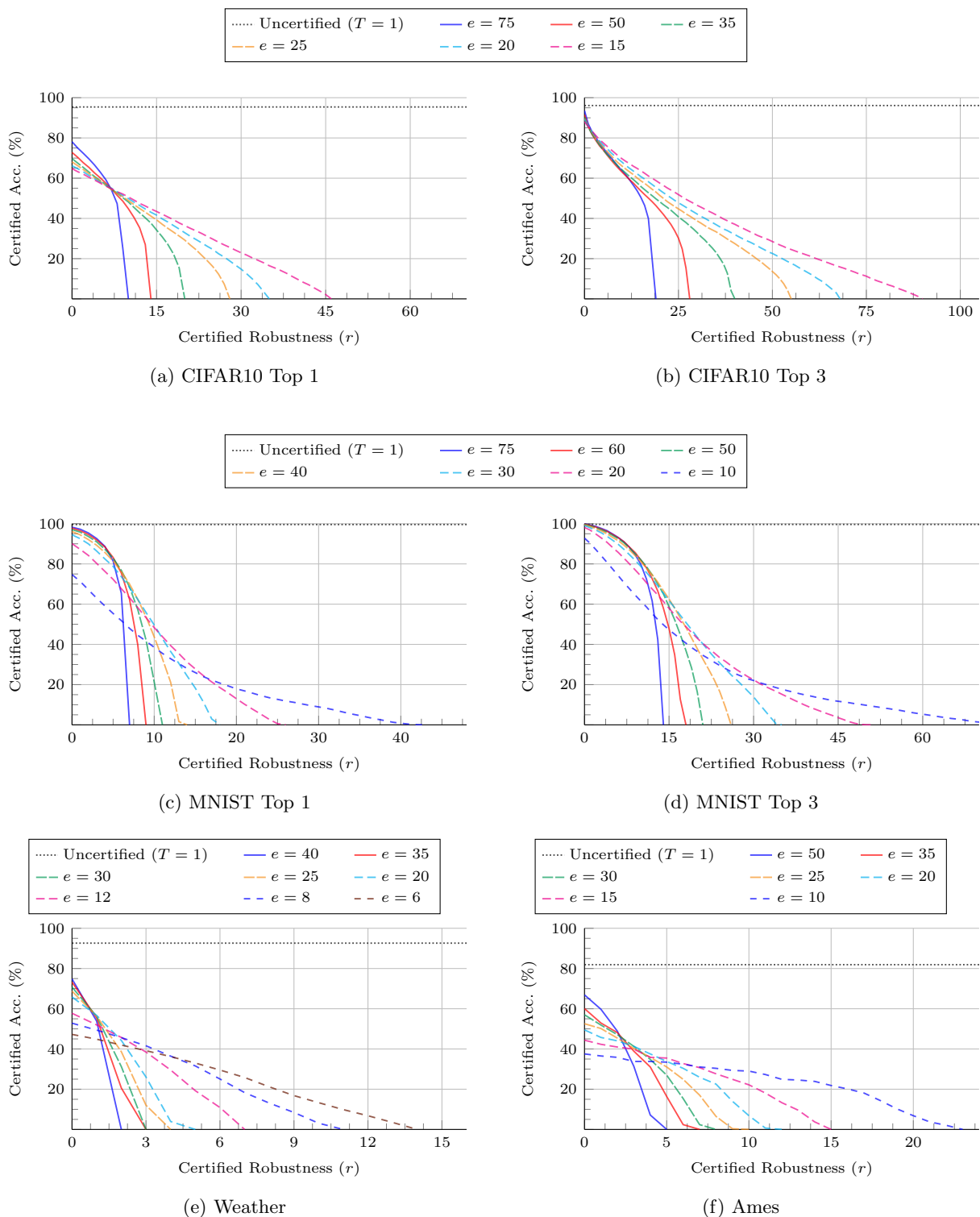


Figure 9: **Effect of the Number of Kept Features (e) on Certified ℓ_0 -Norm Robustness:** Mean certified accuracy for baseline randomized ablation across different quantities of kept pixels (e). Uncertified accuracy (.....) visualizes the peak accuracy of a single model ($T = 1$) trained on all features; these single model predictions are completely non-robust and provided only for reference.

F.5 Random vs. Deterministic Feature Partitioning

Sec. 5 proposes two paradigms for partitioning the d features between the T submodels. The first option, *balanced random partitioning*, assigns each submodel approximately the same number of features uniformly at random. The second option, *deterministic partitioning*, uses a deterministic scheme to decide which features are assigned to the same submodel.

In the main paper, we propose what we term “strided partitioning,” a deterministic partitioning strategy where for submodel f_t , the corresponding feature set is

$$\mathcal{S}_t = \{j \in [d] : j \bmod d = t\}. \quad (34)$$

Strided partitioning is specifically targeted toward structured, two-dimensional feature sets (e.g., images). Striding ensures that each subset \mathcal{S}_t contains feature information across the 2D grid.

Alternative deterministic strategies we considered include “patching,” where the image is broken up into a grid of disjoint 2D patches. Each submodel is then trained on a different subpatch. Patching performed exceptionally poorly (much worse than random partitioning) because, in short, each submodel is trained on highly correlated pixels limiting the information available to each. Moreover, many of the submodel patches contained no information from the highly salient center pixels.

A third deterministic partitioning strategy we considered assigned pixels to each submodel starting from the center of the image. In essence, this “spiral” strategy renumbers the pixels defining the center pixel as feature 1 and then assigning pixels indices in order based on their Manhattan distance from this pixel. The intuition behind the “spiral” strategy is enforcing the rule that each submodel has access to pixels in the images center.

Figure 10 compares the performance of random partitioning versus the consistently best performing deterministic strategy – striding. We consider three datasets in Sec. 6. First, CIFAR10 [KNH14] ($d = 1024$) and MNIST [LeC+98] ($d = 784$) are image classification datasets while Weather [Mal+21] is a tabular regression dataset. For all three datasets, the partitioning strategy used in Sec. 6 is shown as a solid line, while the other partitioning strategy is shown as a dashed line. Below we briefly summarize the key takeaways from Fig. 10.

Takeaway #1: *Deterministic feature partitioning significantly improves FPA’s performance on vision datasets.* For both CIFAR10 and MNIST, deterministic (strided) feature partitioning significantly outperforms random partitioning. For example, on CIFAR10 and MNIST top 1 predictions with 25 models, strided partitioning improves the mean certified accuracy by up to 15.6% and 11.9%, respectively.

Takeaway #2: *Deterministic partitioning’s benefits decrease with increasing submodel count.* For CIFAR10 with $T = 115$ submodels, deterministic partitioning improved FPA’s mean certified accuracy by at most 5.8%; in contrast, for CIFAR10 with $T = 25$ submodels, deterministic partitioning improved performance by up to 15.6%. A similar trend is observed for MNIST. As T increases, each submodel is trained on (substantially) fewer pixels. As feature sparsity increases, the benefit of a regular pixel pattern decreases.

Takeaway #3: *Deterministic and random partitioning perform comparably for the Weather dataset.* Tabular features are generally unstructured or, in some cases, loosely structured. Intuitively, there is not a consistent advantage in ensuring that the tabular features considered by each submodel are well-spaced. A deterministic tabular feature partition can be viewed as a random variable drawn from the set of all random partitions. Some deterministic partitions will outperform the mean random partition; other deterministic partitions will underperform the mean random partition. We see this behavior in Fig. 10e, where for $T = 11$, strided partitioning outperforms balanced random while for $T = 21$, balanced random is better. For $T = 31$, strided and random partitioning perform similarly.

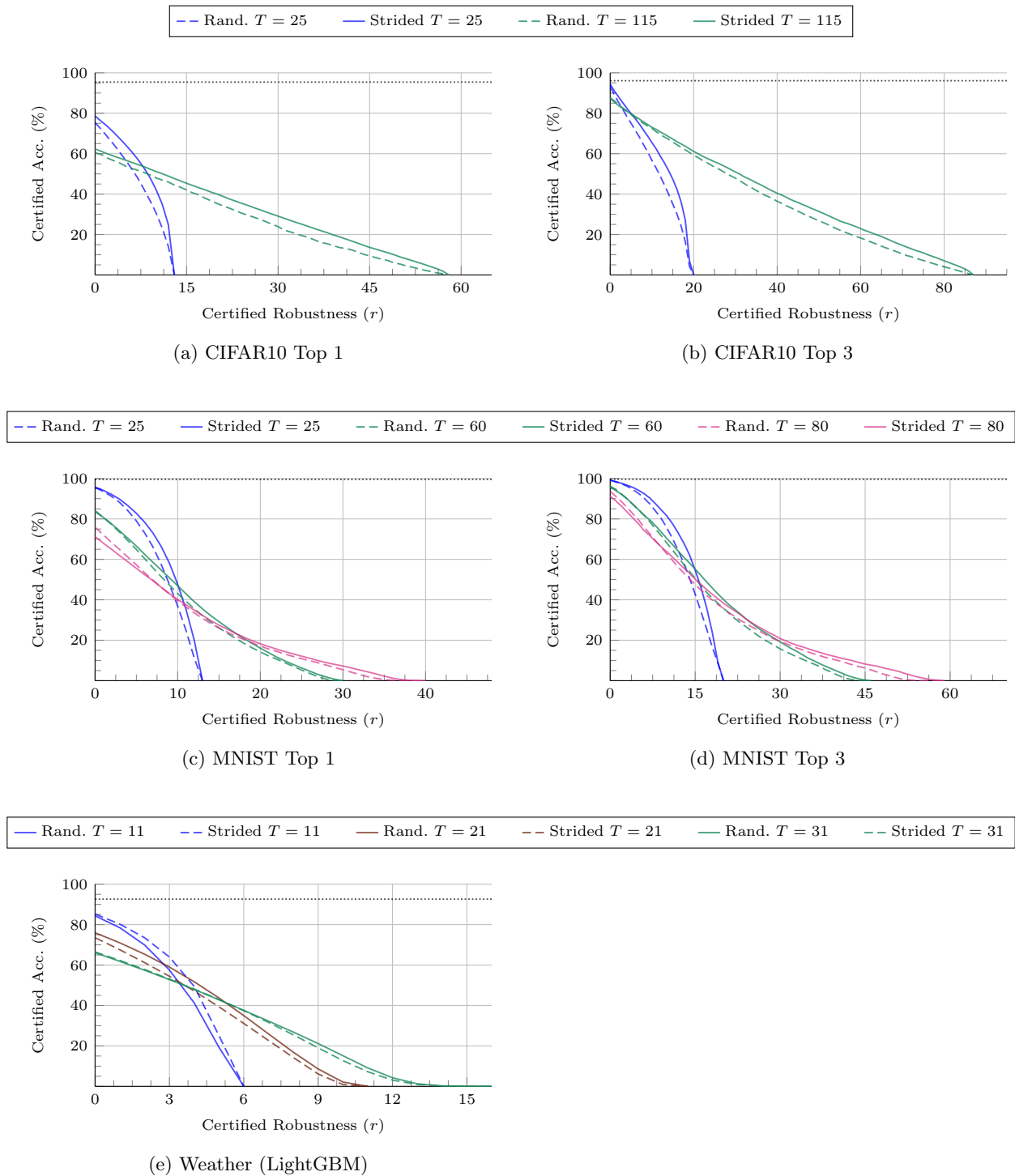


Figure 10: **Effect of the Feature Partitioning Paradigm on Certified Feature Robustness:** Mean certified accuracy for feature partition aggregation across different feature partitioning paradigms. Uncertified accuracy (.....) visualizes the peak accuracy of a single model ($T=1$) trained on all features; these single model predictions are completely non-robust and provided only for reference. For each dataset, the feature partitioning strategy used in Sec. 6 is shown as a solid line. The alternate feature partitioning strategy is shown in the same color but as dashed lines.

F.6 Model Training Times

This section summarizes the model training times of feature partition aggregation (FPA) and baseline randomized ablation (RA). These experiments were performed on a desktop system with a single AMD 5950X 16-core CPU, 64GB of 3200MHz DDR4 RAM, and a single NVIDIA 3090 GPU.

Recall that certified defenses against sparse attacks – both ours and randomized ablation – trade off accuracy against robustness. Put simply, larger certified guarantees are generally achieved at the expense of reduced accuracy (and vice versa). To capture the nature of this tradeoff, Sec. 6.2 reports performance for two versions of the baseline – a higher accuracy version that “keeps” more pixels per iteration (i.e., ablates fewer features) and a more robust version that keeps fewer features (i.e., ablates more features). To ensure a more direct comparison, Sec. 6.2 similarly reports results for higher accuracy as well as more robust versions of our method FPA.

Table 26 reports the mean training time for the higher accuracy and more robust versions of FPA and randomized ablation. For FPA, we separately report the mean training time for a single submodel (e.g., f_t) as well as the total training time of the entire ensemble (f). Model training for randomized ablation used Levine and Feizi’s [LF20] original source code for MNIST and CIFAR10. Levine and Feizi’s code was modified to support the Weather and Ames datasets, which are not included in RA’s published implementation.

For the tabular Weather and Ames dataset, FPA was $18\times$ to $90\times$ faster to train than randomized ablation. Randomized ablation is only compatible with model types that support stochastic, ablated training. By contrast, FPA supports any submodel type, including LightGBM gradient-boosted decision trees (GBDTs) used here. For Weather and Ames, GBDTs are both faster to train and more accurate than ablated linear models.

For vision datasets MNIST and CIFAR10, FPA’s total ensemble training times are $2.1\times$ to $11\times$ slower than randomized ablation. Note that the training of each FPA submodel is fully independent. In other words, FPA ensemble training is embarrassingly parallel with up to T degrees of parallelism. Provided sufficient hardware, an FPA ensemble can be (significantly) faster to train in parallel than a randomized ablation model, as evidenced by Tab. 26’s single FPA submodel training times.

Table 26: **Model Training Time:** Mean model training time (in seconds) for feature partition aggregation (FPA) versus baseline randomized ablation. For each dataset, Sec. 6.2 considers two variants of each defense – one that achieves higher certified accuracy and the other that achieves larger certified robustness. Below we report the model training times for both variants. For FPA, the time to train a single submodel and the total time to train the entire ensemble are reported. “<1” denotes that training took less than 1 second.

| Dataset | Random. Abl. | | FPA (ours) | | |
|---------|--------------|-------|------------|--------|--------|
| | e | Time | T | Single | Total |
| CIFAR10 | 75 | 6,278 | 25 | 541 | 13,526 |
| | 25 | 6,085 | 115 | 544 | 62,613 |
| MNIST | 45 | 904 | 25 | 153 | 3,834 |
| | 20 | 883 | 60 | 161 | 9,669 |
| Weather | 20 | 5,186 | 11 | 13 | 141 |
| | 8 | 5,210 | 31 | 9 | 278 |
| Ames | 50 | 63 | 11 | <1 | 1 |
| | 15 | 64 | 51 | <1 | <1 |